Long-term ecosystem dynamics of an ice-poor permafrost peatland in eastern Eurasia: paleoecological insights into climate sensitivity

Zhengyu Xia[1,*], Fengtong Chen[1,*], Mengyang Guo[1], Zicheng Yu[1,2]

[1]Key Laboratory of Geographical Processes and Ecological Security in Changbai Mountains, Ministry of Education, School
of Geographical Sciences, Northeast Normal University, Changchun, 130024, China
[2]State Key Laboratory of Black Soils Conservation and Utilization, Northeast Institute of Geography and Agroecology,
Chinese Academy of Sciences, Changchun, 130102, China
[*]These authors contributed equally to this work

Correspondence to: Zicheng Yu (yuzc315@nenu.edu.cn), Zhengyu Xia (zhyxia@hotmail.com)

Abstract. Northern peatlands are carbon-rich ecosystems highly sensitive to climate change, with nearly half of their carbon stocks associated with permafrost. Peat-based paleoecological records provide insights into the complex responses of permafrost peatlands to long-term climate variability, but most studies were conducted in ice-rich permafrost peatlands in Europe and North America. Here, we use multiple active-layer cores to reconstruct the ecosystem history of an ice-poor permafrost peatland in eastern Eurasia, near the southernmost limit of circumpolar permafrost but outside the circumpolar thermokarst landscape.

Our results show that the peatland, which developed on a floodplain since the late Holocene cooling, underwent a major phase of lateral expansion during the Little Ice Age. A fen-to-bog transition occurred in recent decades, with dry-adapted *Sphagnum* mosses replacing herbaceous vegetation across the site and having rapid surficial peat accumulation. Carbon isotope ratios of *Sphagnum* macrofossils, a proxy for surface wetness, indicate that *Sphagnum* mosses initially established under very dry conditions but that their habitats have since become gradually wetter.

Synthesizing these findings, we highlight that: (1) permafrost aggradation during climate cooling may promote new peatland formation over permeable mineral substrate by impeding drainage; (2) anthropogenic climate warming and active layer deepening can induce an ecosystem-scale regime shift, but ice-poor permafrost peatlands generally exhibit stability and homogeneity due to the absence of dynamic surface morphology (such as frost heave and thermokarst collapse); (3) recent wetting may result from surface adjustment–hydrology feedback and vegetation–hydrology feedback, demonstrating the internally driven resilience of ice-poor permafrost peatlands in maintaining their hydrology and carbon accumulation; and (4) ice-poor permafrost peatlands are likely to remain persistent carbon sinks under ongoing and future climate change.

1 Introduction

Northern peatlands are globally important and persistent carbon (C) sinks over time (Gorham, 1991; Yu et al., 2011; Treat et al., 2019), with the size of their C stocks estimated to be 400–500 Pg C (Yu, 2012; Hugelius et al., 2020). Almost

half of the northern peatland C is affected by circumpolar permafrost (Smith et al., 2007; Hugelius et al., 2020). This biosphere-cryosphere interaction renders permafrost peatlands—commonly found in northern high latitudes—highly sensitive to ongoing warming and permafrost degradation, which, beyond the simple thawing process, entails compound changes in surface morphology, hydrology, soil structure, vegetation composition, and erosion regime (Payette et al., 2004; O'Donnell et al., 2012; Borge et al., 2017; Olefeldt et al., 2021; Errington et al., 2024). There is a growing concern that degradation of C-rich permafrost peatlands may trigger strong C-cycle feedback that will further accelerate climate warming in the future (Schneider von Deimling et al., 2012; Turetsky et al., 2020).

Permafrost peatlands are heterogeneous landscape features dominated by diverse landforms across permafrost zones (Zoltai and Tarnocai, 1975; Vitt et al., 1994). For example, perennial frost mounds such as palsas or peat plateaus are found in the boreal zone, whereas ice-wedge polygons are found in the Arctic tundra zone (Treat et al., 2016; Olefeldt et al., 2021). These landforms are not always in equilibrium with the climate (Camill and Clark, 1998; Vitt et al., 2000) and may undergo multiple and locally inconsistent stages of transition in response to permafrost degradation (Swindles et al., 2015; Hugelius et al., 2020; Olefeldt et al., 2021), forming new lakes, ponds, fens, and bogs. Generally, field-based greenhouse gas flux measurements and laboratory-based incubation or mesocosm experiments indicate that decomposition of previously frozen organic matter (OM), once upon thaw, has the potential to increase emissions of both CO_2 and CH_4 (and N_2O) (Turetsky et al., 2002; Hodgkins et al., 2014; Voigt et al., 2017; Voigt et al., 2019). Direct measurements of belowground C stocks across chronosequence also present evidence for possibly substantial losses of organic C following thaw and surface collapse (O'Donnell et al., 2012; Jones et al., 2017; Harris et al., 2023). However, these studies yield highly diverse results, due to methodological biases, regional variations (permafrost history and peat type), and local processes (geomorphic setting and hydrology) (Treat et al., 2014; Cooper et al., 2017; Estop-Aragonés et al., 2018; Knoblauch et al., 2018; Heffernan et al., 2020; Manies et al., 2021; Heffernan et al., 2024). Therefore, predicting the future fate and trajectory of C stored in permafrost peatlands as well as their climate feedback relies on empirical equilibrium models due to spatiotemporal complexities inherent to such systems (Hugelius et al., 2020; Turetsky et al., 2020; Treat et al., 2021; Fewster et al., 2022).

Paleoecological records derived from peatland archives offer crucial insights into how permafrost peatlands respond to climate variability during their own development histories and are particularly relevant to understanding the slow changes of and interactions among climate, permafrost, hydrology, vegetation, disturbance, and C accumulation on decadal to millennial timescales (Camill et al., 2009; Bauer and Vitt, 2011; Hunt et al., 2013; Jones et al., 2013; Swindles et al., 2015; Gałka et al., 2017; Xia et al., 2024a). Among boreal peatlands, multiple records document that permafrost aggradation during Holocene climate cooling resulted in elevated and drier peatland surfaces, with an increased abundance of bog-like vegetation (shrubs and *Sphagnum* mosses), more frequent and severe wildfires, and decreased C accumulation rates (Robinson and Moore, 2000; Oksanen et al., 2001; Turetsky et al., 2007; Hunt et al., 2013; Treat et al., 2016). During the current warm period with permafrost thaw, high-resolution proxy records show diverse ongoing ecohydrological trajectories, with some shifting drier due to deeper active layers or higher evapotranspiration rates, some shifting wetter due to accelerated thaw or surface collapse, and some experiencing fluctuating conditions (Zhang et al., 2022). These diverse

65 trajectories had different impacts on peatland C accumulation rates (Swindles et al., 2015; Zhang et al., 2018a; Sim et al., 2021). Moreover, there is growing evidence of vegetation shift in recently drying permafrost peatlands toward the dominance of *Sphagnum* mosses (Magnan et al., 2018; Taylor et al., 2019; Chartrand et al., 2023; Piilo et al., 2023; Cleary et al., 2024), a well-known "peat builder" that may enhance the C sink capacity through multiple mechanisms (Clymo and Hayward, 1982; van Breemen, 1995).

70   Despite the progress to date, it is noteworthy that the current literature and relevant knowledge about the histories and present states of permafrost peatlands are disproportionately built on studies carried out across ice-rich permafrost environments in Europe and North America. Conversely, there are very few counterpart records documented from eastern Eurasia (Treat et al., 2016), which encompasses a vast area and a further southward, inland distribution of circumpolar permafrost (Fig. 1a). Therefore, our understanding of the processes and mechanisms governing the response of permafrost
75 peatlands to climate change may be incomplete.

        Northern Northeast China is situated at the southernmost limit of circumpolar permafrost (Fig. 1b). The regional permafrost is highly sensitive to natural and anthropogenic drivers, with degradation being widely documented over recent decades (Jin et al., 2000). Although peatlands are abundant in this region (Xing et al., 2015), only a limited number of sites have been thoroughly described and investigated so far. These studies mostly focused on greenhouse gas fluxes (Miao et al.,
80 2012a; Yu et al., 2017; Sun et al., 2024), biogeochemical cycling (Wang et al., 2010; Guo et al., 2018; Ramm et al., 2022), and C accumulation patterns (Xing et al., 2015; Liu et al., 2019a), or use peatlands as archives for reconstructing past wildfire, dust, and pollution histories (Bao et al., 2012; Bao et al., 2014; Gao et al., 2018). Only a few studies aimed to explicitly examine their long-term ecosystem histories using peat-core analysis (Liu et al., 2024b; Xia et al., 2024a). Furthermore, despite the presence of permafrost, this region is not within the circumpolar thermokarst landscape (Fig. 1a)
85 due to the underlying ice-poor conditions (Brown et al., 1997; Jin et al., 2016; Olefeldt et al., 2016). Regional peatlands barely show ground expansion- or collapse-related surface terrain characteristics, unlike those ice-rich European and North American permafrost peatlands extensively described in the literature (Olefeldt et al., 2021). Therefore, it remains unclear whether and how climate-permafrost dynamics affect regional peatlands, or whether such dynamics differ from other permafrost regions.

90
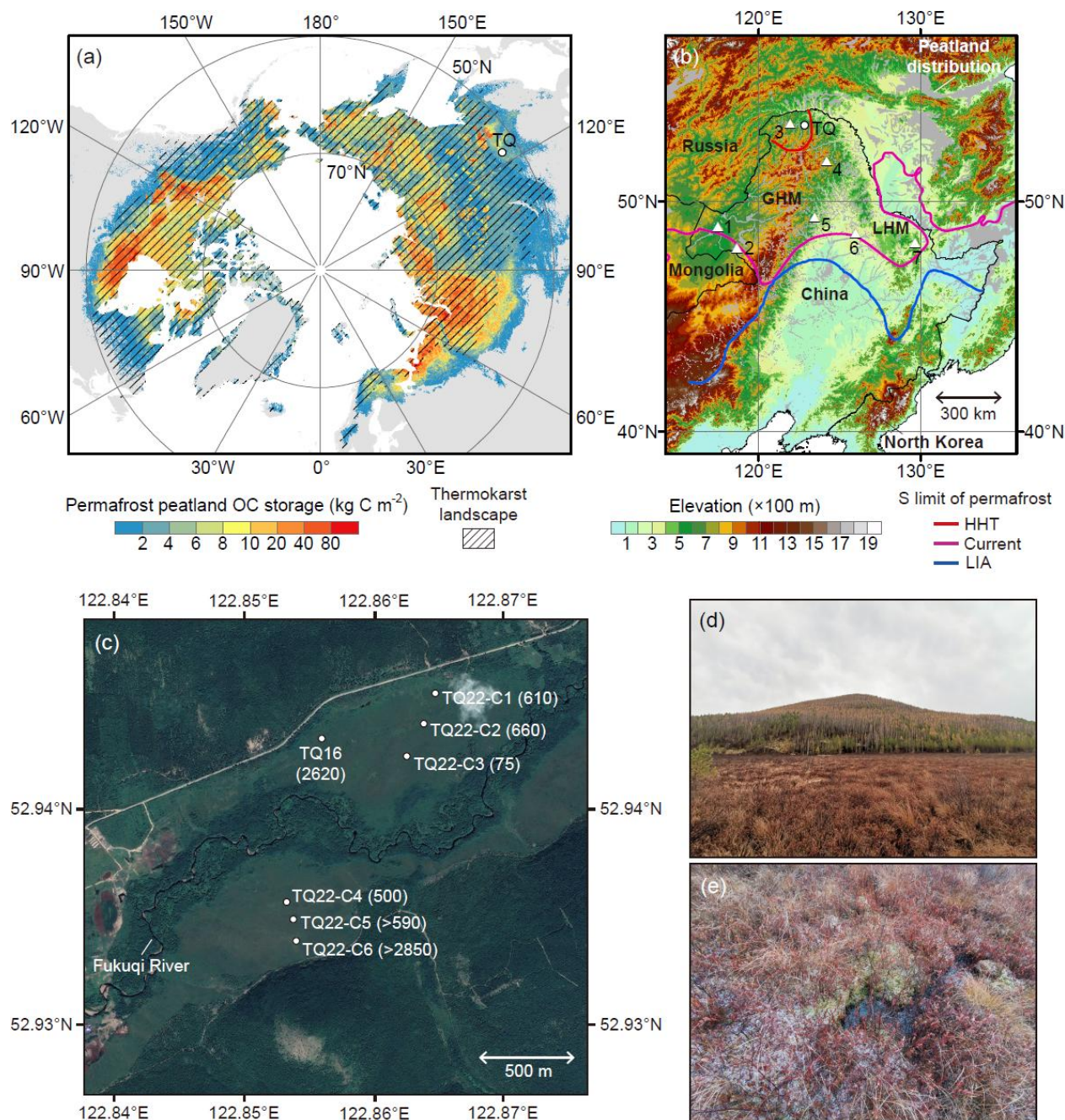
Figure 1. Overview of the study region and site. (a) Circumpolar map of permafrost peatland organic carbon (OC) storage from Hugelius et al. (2020), overlain by thermokarst landscape distribution from Olefeldt et al. (2016) in hatched areas and the location of Tuqiang (TQ) peatland—our study site. (b) Map of Northeast China showing elevation, the distribution of peatlands or peat-forming wetlands (Xu et al., 2018), the location of Tuqiang peatland, the location of other paleoclimate records later mentioned in this paper (1—Hulun Lake; 2—Yihesariwusu Lake; 3—Huola Basin; 4—Hongtu Peatland; 5—

Sifangshan Lake; 6—Tianchi Crater Lake; 7—Tanghongling Mire), the current southern limit of permafrost (Brown et al., 1997), and the inferred southern limits of permafrost during the Holocene Hypsithermal period (HHT) and the Little Ice Age (LIA) in China (redrawn from Jin et al., 2000). GHM—Greater Hinggan Mountains; LHM—Lesser Hinggan Mountains. (c) Google Earth aerial image (© Google Earth 2025, CNES/Airbus) of Tuqiang peatland, showing the locations of cores collected in this study (TQ22) and a previous study (TQ16) by Han et al. (2019). The numbers in parentheses indicate peat initiation ages in cal. yr BP. TQ22-C5 and TQ22-C6 did not reach the basal peat, thus peat initiation ages should be earlier than their oldest ages. (d) Field view of Tuqiang peatland (in front of a hill). (e) Typical surface vegetation of Tuqiang peatland (with whitish snowflakes at the time of field sampling in September 2022).

Herein, we aim to address these critical data and knowledge gaps by analyzing peat properties, plant macrofossils, and moisture indicators from six radiocarbon-dated active-layer cores to reconstruct the ecosystem history of a boreal ice-poor peatland within the predominantly continuous permafrost zone in northern Northeast China. Specifically, our objectives are to: (1) determine how peatland formation and development, including long-term changes in ecosystem structure and function, responded to climate variability over long timescales; and (2) understand the role of permafrost in regulating these changes. These objectives are driven by our overarching hypothesis that climate-permafrost interactions and relevant feedback are fundamental in shaping the long-term evolution of peatlands, but due to the absence of dynamic surface morphology (such as frost heave and thermokarst collapse) in ice-poor permafrost environments, the specific processes and mechanisms are expected to differ from those in ice-rich permafrost peatlands. Collecting multiple cores allows us to draw a complete picture of peatland history, capture any spatial heterogeneity, and reduce biases that can arise from relying on a single core.

2 Materials and methods

2.1 Study site and sampling

Our study site is Tuqiang peatland (52.94°N, 122.86°E; elevation 475 m asl) in the northern Greater Hinggan Mountains of Northeast China, near the border with Russia (Fig. 1b). This site is within the "predominantly continuous permafrost" zone based on a national classification (Ran et al., 2012; Zhang et al., 2021), which has been considered more regionally suitable than the "discontinuous permafrost" zone provided by the International Permafrost Association (Brown et al., 1997). From nearby Mohe weather station (1959–2022), the mean annual temperature is –4.1 °C and the mean annual precipitation is 443 mm (365 mm in May–September).

Tuqiang peatland was developed on a floodplain as part of a larger peatland complex extending along the Fukuqi River (Fig. 1c). Peatland vegetation varies with microform features across the site, with hummocks dominated by *Sphagnum* mosses (such as nutrient-poor species *S. magellanicum* and *S. capillifolium*) and Ericaceae shrubs (*Vaccinium uliginosum*, *Ledum palustre*, and *Chamaedaphne calyculata*), and hollows dominated by tussock sedges (*Eriophorum vaginatum*) (Fig.

1e; Miao et al., 2012a; Liu et al., 2024b; Sun et al., 2024). Other notable plant species include *Alnus sibirica*, *Betula*
130 *fruticosa*, *Salix rosmarinifolia*, *Deyeuxia angustifolia*, *Carex* spp., and *Polytrichum* spp. The peatland hydrology is mainly
controlled by precipitation and evapotranspiration fluxes, as well as seasonally changing thaw depth, without obvious
influence from nutrient-rich surface water and groundwater inflows (Liu et al., 2024b; Sun et al., 2024). The maximum thaw
depth is 50–70 cm (Sun et al., 2024). The water table depth generally varies between 10 cm and 35 cm below shrub-moss
hummocks during the growing season, reaching its peak depth in mid-summer if there is no heavy precipitation event, based
135 on previous field monitoring data (Miao et al., 2012a; Liu et al., 2024a).

Tuqiang peatland does not have developed any permafrost-related outstanding surface terrain feature such as palsas,
peat plateaus, thermokarst collapses, or ponds (Fig. 1d). As a nationally well-known site, it has been studied for over a
decade with an eddy covariance tower monitoring greenhouse gas fluxes in the northern section (Yu et al., 2017; Sun et al.,
2024).

140 In September 2022, we collected six active-layer cores from *Sphagnum*-dominated surfaces in Tuqiang peatland
using a stainless serrated knife and a 7×7 cm box corer: three from the northern section and three from the southern section
(Fig. 1c). Their key information is summarized in Table 1. Briefly, two cores, TQ22-C5 and TQ22-C6, did not reach basal
peat and mineral substrate. All cores were stored in the laboratory under frozen conditions.

145 **Table 1.** Key information about collected peat cores from Tuqiang peatland.

Core ID	Latitude (°N)	Longitude (°E)	Core length[a] (cm)	Total peat section length[b] (cm)	*Sphagnum* peat section depth[b] (cm)
TQ22-C1	52.9453	122.8647	57	49	0–16
TQ22-C2	52.9440	122.8639	52	34	0–23
TQ22-C3	52.9425	122.8628	81	43	0–38.9
TQ22-C4	52.9340	122.8540	69	59.3	0–45.7
TQ22-C5	52.9349	122.8537	60	60	0–30
TQ22-C6	52.9357	122.8533	65	65	0–26, 30–41

[a] Measured in the field.
[b] Measured in the laboratory and corrected to match the field depth.

2.2 Laboratory analysis

The collected peatland cores were cut with a band saw in frozen state in the laboratory into 1 cm slices, which were
subsequently subsampled all the analyses. Some core sections had experienced compression or expansion by a few
150 centimeters compared to the original core lengths measured in the field. Therefore, sample depths were corrected if
necessary to match the field-measured core lengths (Table 1).

Physical properties of cores were analyzed at 1 cm intervals following the standard protocol of loss-on-ignition.
Briefly, subsamples of 1 cm³ were dried in an oven at 105 °C for 24 h to measure water content and dry bulk density. Then,

the dried subsamples were burned in a muffle furnace at 550 °C for 4 h to estimate OM content and ash-free bulk density
155 (AFBD). Bulk peat concentrations of C and nitrogen (N) of cores were analyzed at 2 cm intervals for peat sections using an
elemental analyzer (EA3000, EuroVector, Italy).

All cores were analyzed for ^{14}C dates at a few selected horizons. They have one date at the depth contiguous to the
basal peat or the bottom of the available peat (a few centimeters above for TQ22-C1 due the general lack of credible
macrofossil materials), which we refer to as "basal ages" or "oldest ages". All cores also have one close date at the depth
160 interpreted as the onset of *Sphagnum* peat over sedge peat. *Sphagnum* moss fragments or aboveground part of vascular plant
fragments from 1 cm^3 subsamples were separated and concentrated under a stereomicroscope as dating materials, and then
were freeze-dried. Most dating samples (dry weight of >3 mg) were sent to the Keck AMS Carbon Cycle Lab at the
University of California, Irvine (USA), or the Beta Analytic Testing Laboratory (USA), for ^{14}C measurements. Three dating
samples were analyzed at the newly established MICADAS AMS system housed at Northeast Normal University—authors'
165 institution.

Plant macrofossils from cores were analyzed at 1 cm or 2 cm intervals. Briefly, subsamples of 1 cm^3 were immersed
in a 2% NaOH solution for over 6 h, rinsed with distilled water, and then sieved through a 125 µm mesh. The sieved fine
debris is unidentifiable organic matter (UOM). This fraction was measured for volume after transferring to a cylinder. The
unsieved fraction was examined under a stereomicroscope to identify plant macrofossils. Average volume percentages of
170 different plant remain components, including charcoals, were estimated from 20 views. Additionally, random individual
Sphagnum leaves were identified under a compound microscope to the section level (*Sphagnum*, *Acutifolia*, *Cuspidata*, and
Subsecundum), with their respective percentages calculated.

Sphagnum peat sections of cores were analyzed for *Sphagnum* cellulose carbon and oxygen isotopic compositions at
1 cm or 2 cm intervals, which we use as proxies for local environmental changes. Additional 1–2 cm^3 subsamples were used
175 and first treated like macrofossil subsamples. *Sphagnum* stem tissues (about 20–30 shoots in most cases) were further
separated and concentrated after removing their branches under a stereomicroscope. These materials were then extracted for
cellulose following the established protocol of the alkaline bleaching method, including treatments with NaClO$_2$–CH$_3$COOH
and NaOH solutions (Loader et al., 1997; Kaislahti Tillman et al., 2010). Isotopic analyses of homogenized and freeze-dried
cellulose materials were carried out at the Northeast Institute of Geography and Agroecology, Chinese Academy of Sciences,
180 using a continuous-flow isotope ratio mass spectrometer (MAT253, Thermo Fisher Scientific, USA) coupled with an
elemental analyzer (Flash 2000 HT, Thermo Fisher Scientific, USA). By convention, results of isotopic ratios were reported
as δ notation (in per mille) referenced to VPDB (Vienna Pee Dee Belemnite) for δ^{13}C and to VSMOW (Vienna Standard
Mean Ocean Water) for δ^{18}O. The analytical precision (1σ) was about 0.15‰ for δ^{13}C and 0.2‰ for δ^{18}O (Xia et al., 2024b).

2.3 Modeling peat accumulation

185 We utilized a model of peat mass accumulation based on the proportional decay concept (Clymo, 1984; Clymo et
al., 1998) to fit the relationship between near-surface cumulative peat masses and peat ages by combining all ^{14}C-dated

horizons with post-bomb ages (after 1950) from six cores. This practice assumes that near-surface peat accumulations in different cores are controlled by very similar rates of mass input (litter production) and output (rapid aerobic decay) and that peat of post-bomb ages are still in the acrotelm (surface "aerobic layer") and have not yet been transferred to the catotelm

190   (deep "anaerobic layer"). Considering this model allowed us to assess the post-bomb chronology and reasonably reject unrealistic calibrated ages (calibration of post-bomb ages would yield a possible age at before 1963 and other possible age at after 1963). Additionally, this model yielded key parameters fundamental to understanding the control of peatland C balance.

The model assumes that for a given mass of fresh OM m_0 (g cm^{-2}) produced annually per unit area, the decay process per unit time follows:

$$\frac{\mathrm{d}m}{\mathrm{d}t} = -m\alpha \left(\frac{m}{m_0}\right)^x, \qquad (1)$$

where m is mass (g cm^{-2}), t is time (yr), α is the decay coefficient (yr^{-1}), and x is an exponent controlling the recalcitrance effect (Morris et al., 2015). As decay progresses, the actual decay rate, $\alpha(m/m_0)^x$, may either remain constant ($x = 0$) or decrease ($x > 0$) over time, particularly more rapidly with higher x. For a peat column where fresh OM is continually added from the top and decayed OM remains and accumulates over time, the cumulative peat mass (M) can be expressed as the

200   time integral of m:

$$M(t) = \int_0^t m\,\mathrm{d}t = \begin{cases} \frac{m_0(1-e^{-\alpha t})}{\alpha} & \text{if } x = 0, \\ \frac{m_0\left[(1+x\alpha t)^{\frac{x-1}{x}}-1\right]}{(x-1)\alpha} & \text{if } x > 0 \text{ and } x \neq 1, \\ \frac{m_0 \ln(1+\alpha t)}{\alpha} & \text{if } x = 1. \end{cases} \qquad (2)$$

Equation (2) is a more general expression of the mass–age relationship compared to several special cases shown in Clymo et al. (1998). It was utilized to fit the cumulative peat mass and age data using the least squares method, resulting in a potential range of values for m_0, α, and x when combined. The fitting was carried out using an iterative orthogonal sampling

205   technique that takes m_0 and α values from a space of 0–0.2 g cm^{-2} and 0–0.2 yr^{-1} after assigning a particular x value (0–10). The best fit under each x value was accepted only if the coefficient of determination (R^2) was >0.95. A similar fitting practice has been shown by Charman et al. (2013).

In order to interpret peat-core proxy data as time series, we developed age-depth models for the collected cores using piece-wise linear interpolations between dated intervals (Zhang et al., 2018a; Sim et al., 2019; Fewster et al., 2023;

210   Cleary et al., 2024). The way we derived age-depth models is based on the fact that our cores have very rapid accumulation rates of near-surface peat but much slower accumulation rates of deeper peat that cannot be dated in high resolution. This approach contrasts with Bayesian modeling, which needs to incorporate smoothness-related prior information.

2.4 Other data analyses

215   To summarize the pattern of peatland vegetation changes, we performed principal component analysis (PCA) to reduce the dimensionality of the macrofossil data, in which important macrofossil types (mean percentage >1%) were selected and percentage data were log-transformed.

To quantify changes in peatland C capacity, we calculated long-term apparent C accumulation rates (aCAR; alternatively, "LORCA") for entire peat core columns, where the C content for OM is based on the mean value (49.7%) derived from our specific C concentration measurements. These aCAR values represent the net rates of C sequestration

220   during the peat accumulation history and were compared with available net ecosystem C balance (NECB) data derived from contemporary eddy covariance measurements combined with observations (Sun et al., 2024). We did not present depth-specific aCAR data as time series due to the well-recognized artifact of an increasing trend from old to young peat (Young et al., 2019; Young et al., 2021).

3 Results

225   **3.1 Peat properties**

Peat property data are presented in Fig. 2. Among all subsamples of six cores, the OM content varies from 2.1% to 100%, and the AFBD varies from 0.014 g cm^{-3} to 0.311 g cm^{-3}. The OM content profiles show lower values at increasing depth and clearly distinguish the transition from mineral substrate to peat in four cores, which is defined based on the threshold of 30% OM content (Table 1). The AFBD profiles generally show higher values in sedge peat sections than in

230   young *Sphagnum* peat and old mineral substrate sections (macrofossil data are described in a following subsection). The mean OM content is 92.2%, 73.4%, and 7.9%, and the mean AFBD is 0.044 g cm^{-3}, 0.150 g cm^{-3}, and 0.090 g cm^{-3} for *Sphagnum* peat, sedge peat, and mineral substrate, respectively. Among these values, it is noted that the *Sphagnum* peat AFBD is very low and the sedge peat AFBD is very high at our site, compared to the northern peatland database (Loisel et al., 2014).

235   Among all subsamples of six cores, the C/N ratio (mass ratio) of bulk peat varies from 16 to 77. The C/N ratio profiles show maximum values at shallow depths and much lower values in deeper sections. The stratigraphical transitions into very low C/N ratios with greater depths are related to abrupt changes in botanical composition from *Sphagnum* peat to sedge peat in each core. The mean C/N ratio is 49 for *Sphagnum* peat and 23 for sedge peat. Both values are low compared to the northern peatland database (Loisel et al., 2014).

240
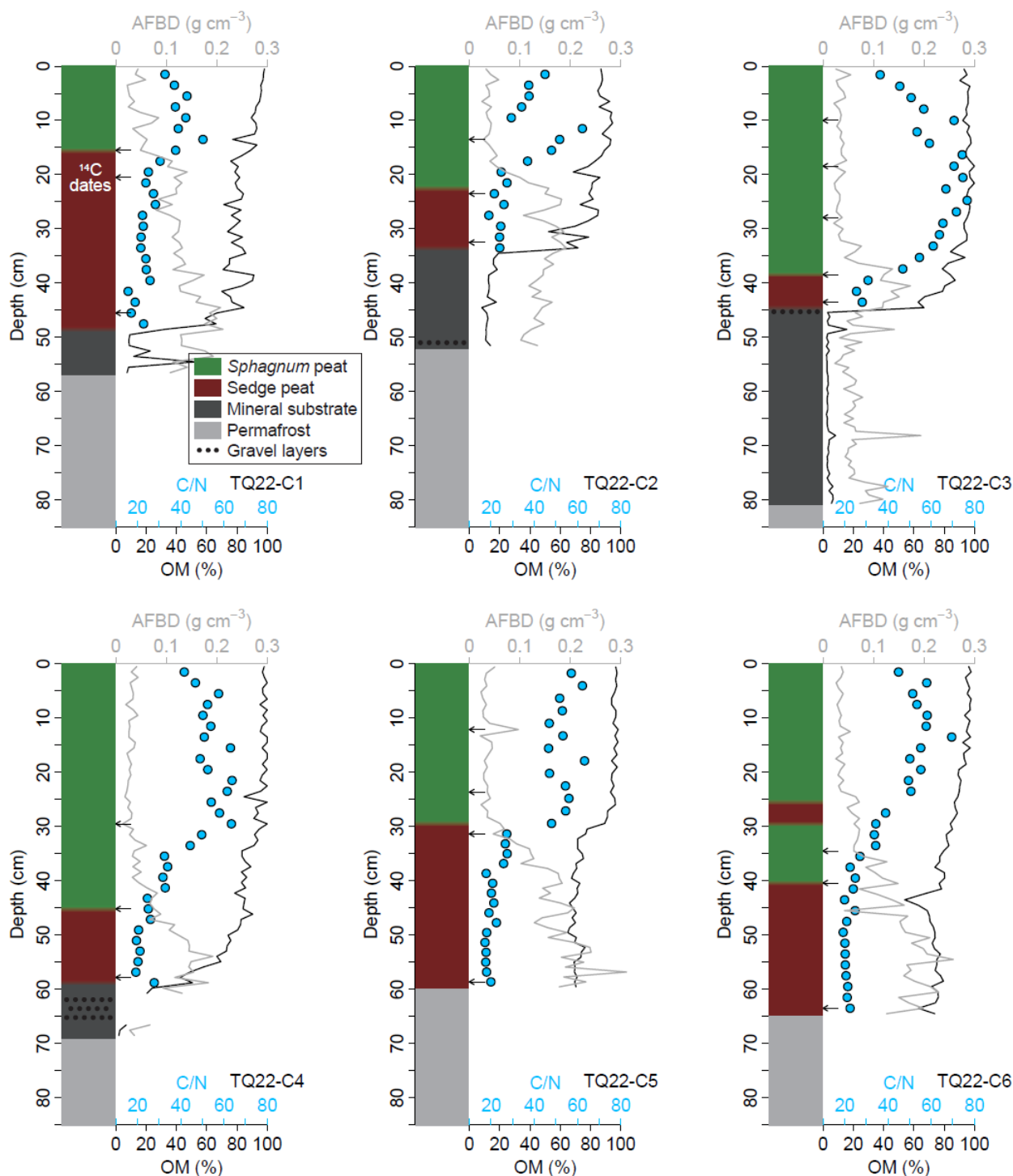
Figure 2. Lithology information and peat properties (organic matter content, ash-free bulk density, C/N ratio) of six cores. Arrows indicate the ^{14}C-dated horizons.

3.2 Radiocarbon dating

Radiocarbon dates and other relevant information are listed in Table 2. We obtained many post-bomb dates, even at >40 cm depth, pointing to very rapid accumulation rates of near-surface peat. The basal ages in median values are 610, 660, 75, and 600 cal. yr BP (equivalent to 1340 CE, 1290 CE, 1875 CE, and 1350 CE) from cores TQ22-C1, TQ22-C2, TQ22-C3, and TQ22-C4, respectively (Fig. 1c). The bottom of available peat in core TQ22-C6 has the oldest date, at a median age of 2850 cal. yr BP.

Table 2. Summary of radiocarbon data from Tuqiang peatland.

Core ID and dated depth (cm)	Lab number	Dated material	"Fraction Modern" ($F^{14}C \pm 1\sigma$) for post-bomb dates or ^{14}C age (^{14}C year BP ± 1σ) for pre-bomb dates	Two possible ages (CE) for post-bomb dates or calibrated age range (cal. year BP, 2σ) for pre-bomb dates
TQ22-C1				
15–16	64306.1.1[a]	*Sphagnum* stems/leaves	1.1102±0.0012	1958, 1995[e]
20–21	UCIAMS-281034[b]	*Sphagnum* stems/leaves	1.4707±0.0022	1962–1963[e], 1972–1973
45–46	UCIAMS-286228	Shrub/herb leaves	*605±15*	*646–585, 567–551*
46–47	UCIAMS-281035	Shrub/herb leaves	1.0961±0.0029[d]	1957–1958, 1998–2001
TQ22-C2				
13–14	UCIAMS-281036	*Sphagnum* stems/leaves	1.0229±0.0015	1955, 2014–2016[e]
23–24	64307.1.1	Shrub/herb parts and *Sphagnum* stems/leaves	1.0088±0.0011	1954–1955[e], 2018
32–33	UCIAMS-281037	Shrub/herb leaves	*710±70*	*770–762, 741–545*
TQ22-C3				
9–10	UCIAMS-286229	*Sphagnum* stems/leaves	1.0232±0.0017	1955, 2014–2016[e]
17–18	UCIAMS-281038	*Sphagnum* stems/leaves	1.0450±0.0015	1956, 2010–2011[e]
26–27	UCIAMS-286230	*Sphagnum* stems/leaves	1.0869±0.0018	1957, 2000–2002[e]
36–37	UCIAMS-281039	*Sphagnum* stems/leaves	1.1117±0.0017	1958[e], 1995–1997
43–44	UCIAMS-286231	*Sphagnum* stems/leaves	*25±15*	*245–230, 135–116, 60–42*
TQ22-C4				
29–30	UCIAMS-281042	*Sphagnum* stems/leaves	1.0546±0.0018	1956–1957, 2007–2009[e]
45–46	64308.1.1	*Sphagnum* stems/leaves	1.0815±0.0011	1957[e], 2001–2003
58–59	UCIAMS-286232	shrub/herb leaves	*430±15*	*513–480*
TQ22-C5				
10–11	UCIAMS-286233	*Sphagnum* stems/leaves	1.0285±0.0017	1955–1956, 2012–2014[e]
20–21	UCIAMS-286234	*Sphagnum* stems/leaves	1.0523±0.0018	1956, 2007–2010[e]
27–28	UCIAMS-281043	*Sphagnum* stems/leaves	1.1005±0.0016	1957–1958, 1997–2000[e]
57–58	UCIAMS-281044	shrub/herb leaves	*650±20*	*663–628, 594–558*
TQ22-C6				
34–35	UCIAMS-281045	*Sphagnum* stems/leaves	1.3567±0.0020	1962[e], 1975–1976

| 40–41 | Beta-717285[c] | *Sphagnum* stems/leaves | *110±30* | *269–212, 196–189, 149–12* |
| 63–64 | UCIAMS-281046 | shrub/herb leaves | *2760±15* | *2919–2906, 2881–2783* |

[a] Lab number in such format means that the sample was analyzed at Northeast Normal University, China.
[b] Lab number with UCIAMS: analyzed at the Keck-CCAMS Laboratory at the University of California, Irvine, USA.
[c] Lab number with Beta: analyzed at the Beta Analytic Testing Laboratory, USA.
[d] Rejected outlier date.
[e] Selected age based on the stratigraphic order or the mass–age relationship.

3.3 Modeled peat accumulation

Figure 3a shows the biplot between cumulative peat masses and calibrated ages of post-bomb dates. By considering the stratigraphic order and the expected concave pattern of the mass–age relationship, we determined, for each post-bomb date, which of the two calibrated ages should be rejected, and then can accept the other one as the most likely age for that dating horizon. However, we cannot definitively determine the correct ages for two post-bomb dates: 20–21 cm of TQ22-C1 and 34–35 cm of TQ22-C6. For these dates, calibration yielded two ages that are close to each other, making it difficult to determine which is more reasonable (Fig. 3a and Table 2). We accepted their older calibrated ages due to being closer to other dates with similar cumulative peat masses.
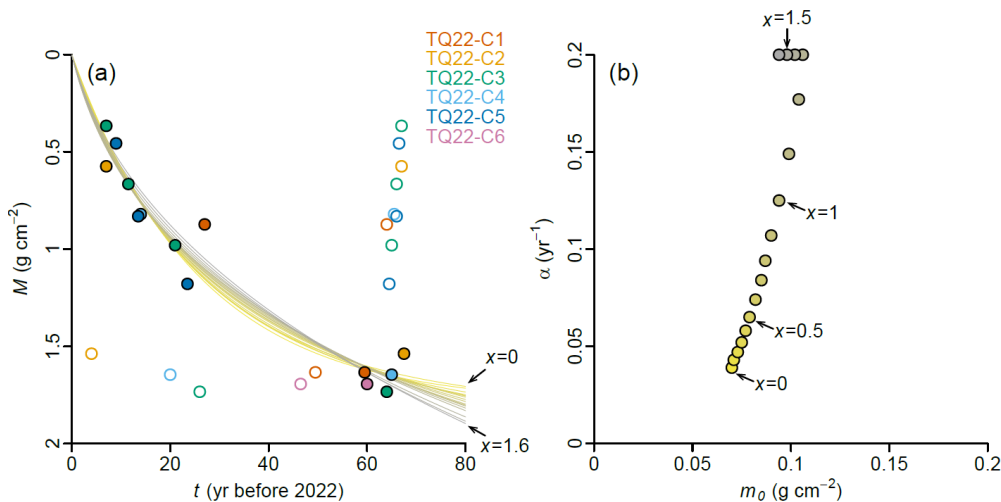
Figure 3. Results of near-surface peat accumulation modeling. (a) The relationship between cumulative peat mass (M) and time (t) derived by combining all post-bomb dates of six cores. Rejected ages after post-bomb calibration are shown as open circles. Accepted ages (closed circles) were fitted using the general expression of Clymo's model, with fitted curves plotted in different colors for different assumptions of recalcitrant effects (x). (b) The fitted values of annual production m_0 and decay coefficient α under different x values.

Combining all these accepted calibrated post-bomb ages, we fitted the mass–age relationship using the general expression of peat decomposition model (Equation 2) and found that the fitted curves can be robust for a wide range of recalcitrance up to $x = 1.6$ (Fig. 3a), in which stronger recalcitrance requires higher rates of production and decomposition (Fig. 3b). The choice of $x = 0.8$ (assuming an intermediate recalcitrant effect) produced the highest fit ($R^2 = 0.962$), with m_0

275 $= 0.087$ g cm^{-2} and $\alpha = 0.094$ yr^{-1}. Assuming no recalcitrant effect would yield $m_0 = 0.07$ g cm^{-2} and $\alpha = 0.039$ yr^{-1} ($R^2 = 0.959$), both of which are higher than reported values from the acrotelm of other northern peatlands (Yu et al., 2001; Loisel and Yu, 2013).

3.4 Plant macrofossil records of peatland vegetation changes

Full plant macrofossil diagrams are presented in Figs. A1–A6. Macrofossil analysis reveals transitions from lower

280 sedge (Cyperaceae) peat to upper *Sphagnum* peat in all cores, although cores TQ22-C1 and TQ22-C6 exhibit somewhat fluctuating abundances of Cyperaceae and *Sphagnum* macrofossils across the transition. We define the onset of *Sphagnum* peat over sedge peat in each core as the greatest depth where *Sphagnum* macrofossils exceed 40% abundance (Table 1 and Fig. 2). The chronology of this stratigraphical transition is well constrained in all six cores. The median ages are 1995 CE, 1955 CE, 1958 CE, 1957 CE, 2001 CE, and 1838 CE, respectively.

285 PCA analysis identifies the statistical relationship among different macrofossil types (Fig. 4a). The first component explains 31.1% of variance and separates the contrasting environmental preferences between dry-adapted *Sphagnum* mosses (sections *Sphagnum* and *Acutifolia*) and wet-favoring herbaceous taxa (Cyperaceae). However, charcoal fragments, which are often interpreted as a drought indicator, are tightly associated with herbaceous taxa. The second component explains 12.1% of variance and separates non-*Sphagnum* mosses and Ericaceae, likely related to microhabitat conditions. PC1 score shows a

290 trend of gradual increase since several hundred years ago, followed by an abrupt increase during the recent century related to the onsets of *Sphagnum* peat accumulation (Fig. 4b).
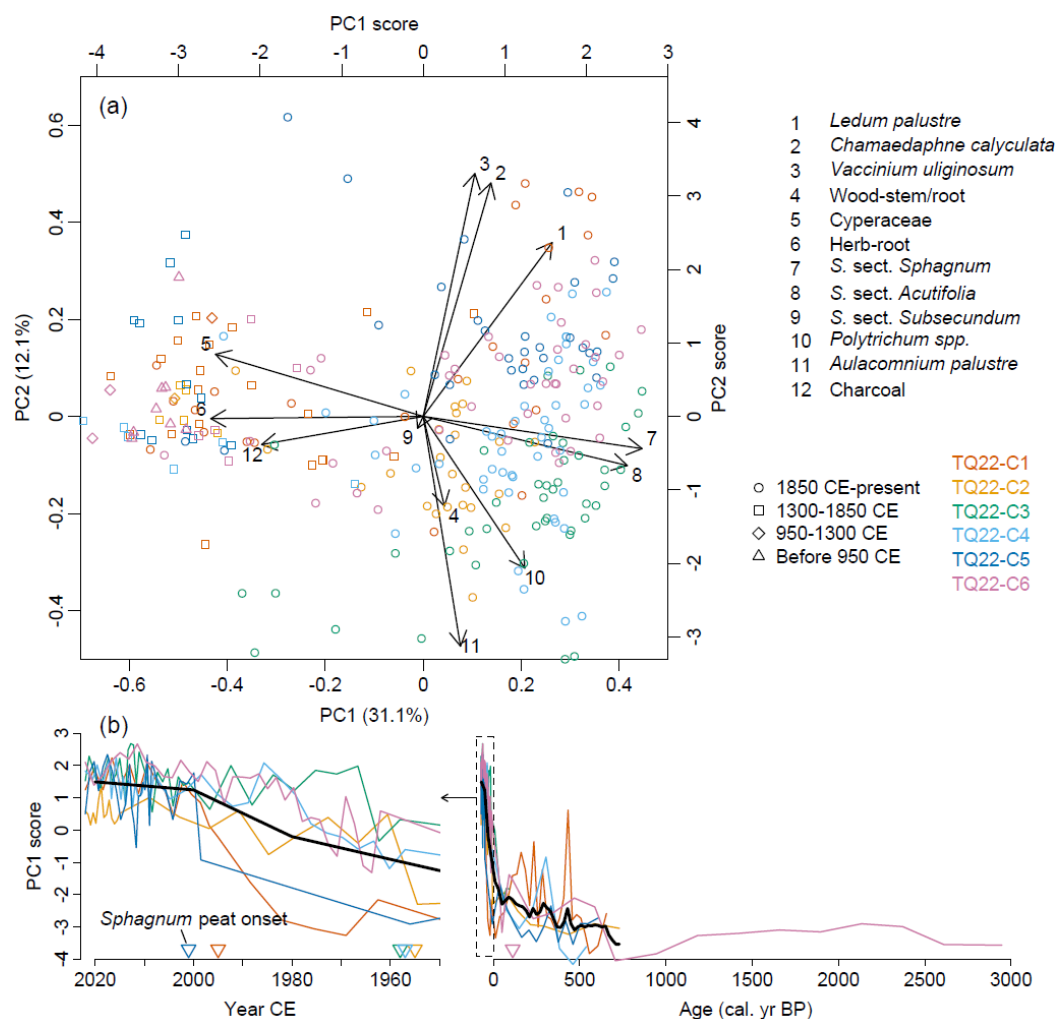
Figure 4. Results of principal component analysis of macrofossil dataset. (a) Component loadings of variables and scores of samples. (b) Changes in PC1 score from different cores with a close-up view of the last 70 years. The black line is the 20-year mean of all individual cores. The onsets of *Sphagnum* peat are marked on the *x*-axis.

3.5 Apparent peat carbon accumulation rates

The long-term aCAR for six cores show an age-dependent pattern with the highest aCAR (163.8 g C m^{-2} yr^{-1}) found in the youngest core, TQ22-C3, and the lowest aCAR (10.4 g C m^{-2} yr^{-1}) found in the oldest core, TQ22-C6 (Fig. 5). The other four cores are of similar ages (660–500 cal. yr BP) but still have highly variable aCAR (24.3–51.2 g C m^{-2} yr^{-1}), showing within-site heterogeneity in the rate of C sequestration. In comparison, the currently available NECB at the same site (Fig. 5), derived mostly from atmospheric C flux measurements, indicates a further higher rate of C sequestration at

about 55 g C m^{-2} yr^{-1} and 74.2 g C m^{-2} yr^{-1} in 2016 and 2017, respectively (Sun et al., 2024), after additionally accounting

305   for the small fluvial C losses of 4.7 g C m^{-2} yr^{-1} (Guo et al., 2018).
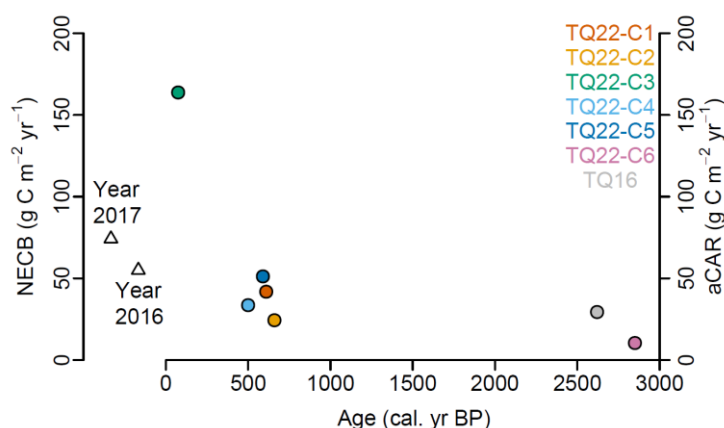
Figure 5. The C sink capacity of Tuqiang peatland. Long-term apparent C accumulation rates (aCAR) of cores collected in this study (TQ22) and a previous study (TQ16) by Han et al. (2019) are plotted against the ages of their basal peat or the
310   bottom of available peat. The annual net ecosystem C balance (NECB) values for the years 2016 and 2017 (Guo et al., 2018; Sun et al., 2024) are plotted on the left side for comparison.

3.6 Isotopic records of environmental changes from *Sphagnum* peat sections

Among all cores, *Sphagnum* cellulose $\delta^{13}C$ ($\delta^{13}C_{cell}$) values range from –32.9‰ to –27.9‰ and cellulose $\delta^{18}O$
315   ($\delta^{18}O_{cell}$) values range from 14.1‰ to 20.2‰. We applied a correction for the "Suess effect" using the method by Leuenberger (2007), which removed the effect of changing $\delta^{13}C$ values of atmospheric CO_2 due to fossil fuel combustion in recent centuries. The "Suess effect"-corrected $\delta^{13}C_{cell}$ values range from –31.7‰ to –25.9‰. Hereafter, $\delta^{13}C_{cell}$ data mentioned in this paper all refer to their corrected values.

The $\delta^{13}C_{cell}$ records show long-term increasing trends with weak fluctuations since *Sphagnum* mosses became the
320   dominant vegetation in three cores: TQ22-C2, TQ22-C3, and TQ22-C5 (Fig. 6b). However, their increasing trends are not synchronous among different cores. Specifically, the $\delta^{13}C_{cell}$ values of TQ22-C3 increase during the period 1960–1990 and remain stable after that, whereas the $\delta^{13}C_{cell}$ values of TQ22-C2 increase during the entire period of 1960–2020. The $\delta^{13}C_{cell}$ values of TQ22-C5 increase after the 2000s. In the other three cores, the $\delta^{13}C_{cell}$ records do not have clear long-term trends but show weak signs of slightly increasing trends in cores TQ22-C1 during the recent decade and TQ22-C6 since the 1970s
325   (Fig. 6b).
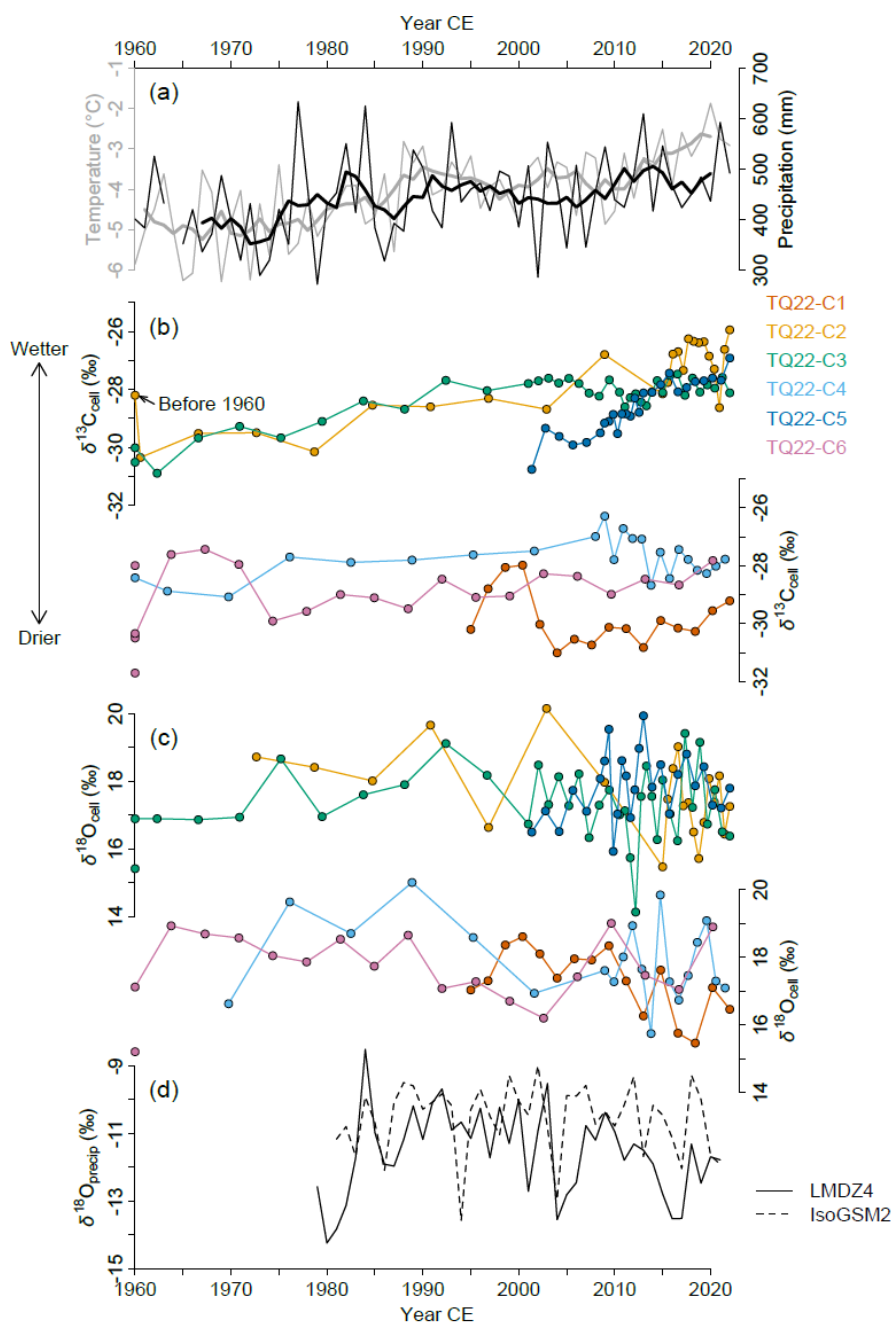
Figure 6. Isotopic records of environmental changes from the period 1960–2022 from high-resolution near-surface peat of six cores. (a) Annual temperature and precipitation records from Mohe weather station, located about 24 km from the Tuqiang peatland. (b) "Suess effect"-corrected *Sphagnum* $\delta^{13}C_{cell}$ records plotted separately for three cores showing progressively wetter conditions (higher $\delta^{13}C_{cell}$) and three other cores that do not show clear long-term trends. Data from earlier periods (before 1960) are plotted along the left *y*-axis. (c) Similar to (b) but for *Sphagnum* $\delta^{18}O_{cell}$ records. (d)

Amount-weighted mean growing-season (May–September) precipitation δ^{18}O for the location of Tuqiang peatland simulated from two nudged isotope-enabled general circulation models, LMDZ4 (Risi et al., 2010) and IsoGSM2 (Yoshimura et al., 2008), the outputs of which are available from the period 1979–2021.

The δ^{18}O$_{cell}$ records are characterized by large sample-to-sample fluctuations with no long-term trends in all cores (Fig. 6c). This temporal pattern is entirely different from that of the δ^{13}C$_{cell}$ records. Chronological uncertainties arising from overly simplistic age-depth models preclude determining whether those δ^{18}O$_{cell}$ spikes are temporally coherent among different cores or correlating δ^{18}O$_{cell}$ variations with the inter-annual variability of temperature, precipitation, or precipitation δ^{18}O (Fig. 6a, d).

4 Discussion

4.1 Possible climate-driven peatland initiation and lateral expansion

A previous global data synthesis of peatland basal ages revealed that growing-season warming during the last deglaciation and early Holocene is the primary driver for the initiation of the most northern peatland areas by enhancing plant productivity (Morris et al., 2018). However, that study included only a limited number of sites from Northeast China. For our site, Han et al. (2019) obtained a basal age of 2620 cal. yr BP (interpolated from their dates between mineral materials and peat) from its northern section, based on one peat core (TQ16) collected from a location west of ours (Fig. 1c). This is much older than our new basal ages and can be interpreted as the timing of peatland initiation. In the southern section, the oldest age of peat cores collected in this study is 2850 cal. yr BP, but it is not the age of basal peat as we did not reach mineral substrate at this coring location (Fig. 1c). Obviously, basal age data from a single site are insufficient for establishing links with large-scale climate forcing. A previous region-wide and comprehensive data synthesis of Northeast China has revealed that the timing of peatland initiation is spatially variable, with more frequent earlier initiations in warmer, lower-latitude locations (Xing et al., 2015). In northern Northeast China including the Greater Hinggan Mountains relevant to this study and the nearby Lesser Hinggan Mountain region, peatland initiation mainly occurred during the late Holocene (Fig. 7a; Xing et al., 2015).

The Holocene climate variability has been a subject of debate, particularly regarding (1) whether the Holocene is characterized by long-term cooling as documented by proxy records or long-term warming as simulated by climate models (the Holocene temperature conundrum; Liu et al., 2014a); and (2) whether the early Holocene was wetter than the late Holocene across all monsoon-affected Asian regions, based on Asian speleothem δ^{18}O records of monsoon intensity (Wang et al., 2005; Liu et al., 2014b). Fortunately, recent studies based on quantitative reconstructions and model-data comparisons provided a timely constraint, showing that the late Holocene—a period of frequent peatland initiations—was characterized by colder and wetter conditions in northern Northeast China compared to the early Holocene (Fig. 7b, c; Jiang et al., 2024;

Zhang et al., 2025). This is in remarkable contrast to the global pattern of warming-driven peatland initiations (Yu et al.,
365   2010; Morris et al., 2018).
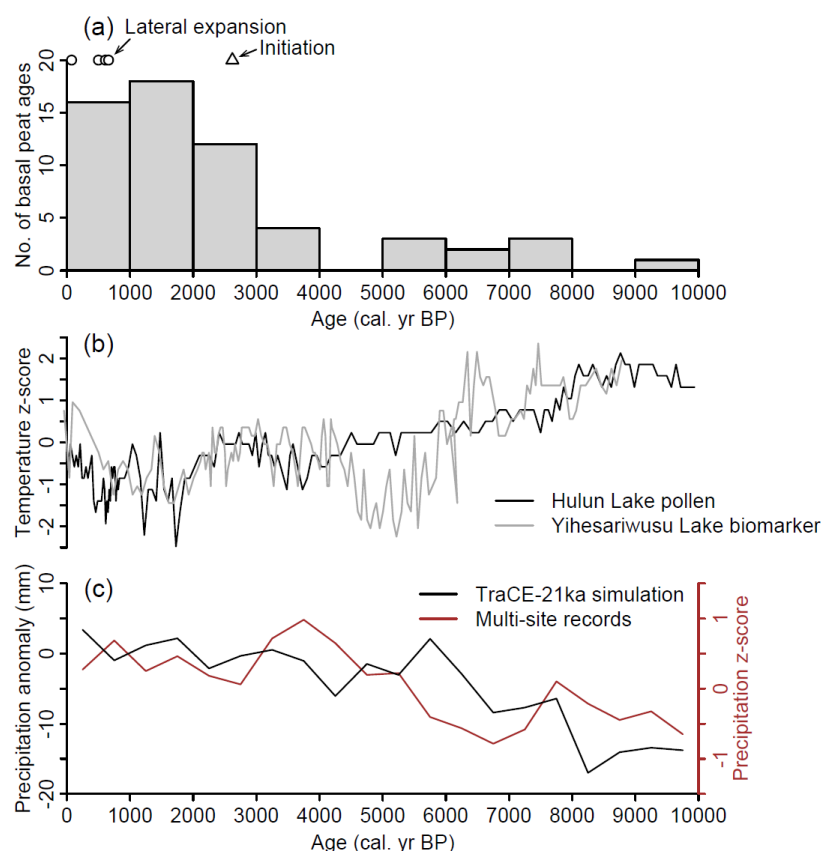
Figure 7. Regional peatland initiation and climate histories during the Holocene. (a) Frequency of basal peat ages from the permafrost-affected Greater Hinggan Mountain and Lesser Hinggan Mountain regions, previously compiled by Xing et al.
370   (2015) and Zhang et al. (2020b). Ages of initiation and lateral expansion of Tuqiang peatland are shown as open triangles and dots. (b) Temperature changes reconstructed using pollen-based transfer function from Hulun Lake (Wen et al., 2010) and using alkenone biomarkers from Yihesariwusu Lake (Jiang et al., 2024). (c) Precipitation changes from a synthesis of multiple proxy records (see Fig. 1b) in northern Northeast China by Zhang et al. (2025), including sites at Huola Basin (Li et al., 2019), Sifangshan Lake (Liu et al., 2017), Tianchi Crater Lake (Zhou et al., 2016; Liu et al., 2019b), and Tanghongling
375   Mire (Yang, 2003), as well as from the model simulation of TraCE-21ka for the same region (Zhang et al., 2025).

Previous data syntheses and many site-specific studies showed that after peatland initiation, the peak period of subsequent lateral expansion in northern peatlands occurred after the Holocene's warmest time, a period that is often referred to as the neoglacial period or late Holocene cooling (Korhola et al., 2010; Weckström et al., 2010; Ruppel et al., 2013; Quik

380 et al., 2023). These studies suggest that lateral expansion might also be climate-driven, with colder and wetter conditions during these periods facilitating the paludification of surrounding mineral soils (Ruppel et al., 2013). For our site, we obtained three (out of six) peat cores that have young basal peat of similar ages (660–500 cal. yr BP), interpreted as indicating a phase of major lateral expansion. The direction of expansion appears to be from upland toward the river channel (Fig. 1c). The timing is within the Ming-Qing cold period in China (1321–1920) that broadly aligns with the Little Ice Age

385 (LIA) (Ge et al., 2013). A recent study using multi-proxy data further suggested that the LIA was characterized by wetter conditions in northern Northeast China (Xia et al., 2024b). Although the lateral expansion of peatlands is poorly documented in our study region, the finding that it occurred at Tuqiang peatland during a climate window of colder and wetter conditions is consistent with the previously identified general pattern in northern peatlands (Ruppel et al., 2013).

Net peat accumulation results from a positive balance between the plant productivity and OM decomposition (Yu et

390 al., 2009). Why are colder and wetter conditions favorable for forming new peatland areas regionally? Superficially, this would suggest that better OM preservation—typically expected under such conditions by slowing down microbial activity— plays the prominent role in initializing and maintaining net peat accumulation. If true, how do we reconcile this finding from the literature that highlights the stronger role of temperature-controlled productivity in shifting the OM balance (Yu et al., 2009; Gallego-Sala et al., 2018; Morris et al., 2018)?

395 A distinct setting of our study region is that peatlands are primarily found on river floodplains and underlain by permafrost. Early surveys noted a spatial overlap between peat-forming wetlands and permafrost in Northeast China, interpreted as evidence for a symbiotic relationship (Sun, 2000). Geological studies mapping past permafrost boundaries showed that Northeast China was nearly permafrost-free during the warmest period of the Holocene, but the permafrost boundary moved southward by approximately 300 km during the late Holocene and the LIA (Fig. 1b; Jin et al., 2000; Jin et

400 al., 2016). This permafrost history provides a framework for our specific hypothesis that the transition from seasonally frozen ground to permafrost might be an agent in regional peatland formation. We propose that permafrost aggradation and its possible expansion toward rivers during cooling periods at our site resulted in thinning active layers and reduced water infiltration. These changes likely triggered feedback mechanisms that enhance poorly drained, waterlogged soil conditions locally (Sun, 2000; Ishikawa et al., 2005; O'Donnell et al., 2012), leading to further better OM preservation than by climate

405 cooling and wetting alone and eventually net peat accumulation (Sun, 2000; Treat et al., 2014).

This hypothesis is based on the fact that Tuqiang peatland developed in a floodplain environment, with gravel/sand-rich sediments observed at the base of cores (Fig. 2). Without permafrost as a physical barrier, rapid and deep drainage through such coarse-grained, highly permeable substrate would prevent soil saturation and also enhance export of dissolved organic C via subsurface flow in a hydrologically connected catchment (Frey and Smith, 2005; Olefeldt and Roulet, 2014;

410 Debolskiy et al., 2021).

Some studies conducted in higher-latitude peatlands noted that permafrost aggradation may result in the assimilation of undecomposed material into frozen ground, leading to the upward accumulation of labile peat concurrent with syngenetic permafrost (O'Donnell et al., 2012; Treat et al., 2016). In this regime, peat may contain cryostructures

(O'Donnell et al., 2012) and often has a very high C/N ratio due to limited C mineralization (Sannel and Kuhry, 2009; Treat

415   et al., 2016). However, neither was observed at our site. The C/N ratio of basal and lower peat sections is only about 25 (Fig. 2), showing no sign of freeze protection compared to >60 in typical permafrost-affected old peat (Treat et al., 2016). The botanical composition of the peat is dominated by sedges, indicating a prolonged status of wet minerotrophic fen in early peatland history (Figs. 2 and A1–A6). These provide support that permafrost aggradation contributed new peat accumulation at our site primarily by maintaining suitable hydrological conditions, rather than by directly freezing the OM.

420   Together, our analysis links the distinct climate drivers of peatland initiation and lateral expansion with permafrost–hydrology feedback, underscoring the importance of considering surficial geology and cryosphere dynamics in understanding the diverse pathways of peatland formation.

4.2 Long-term vegetation and carbon accumulation dynamics

Plant macrofossils preserved in peatland archives have been used as indicators for long-term ecosystem structure
425   shifts (Hughes and Barber, 2004; Camill et al., 2009; Bauer and Vitt, 2011; Treat et al., 2016). For our site, the macrofossil data show long-term stability of wet minerotrophic fen environment dominated by herbaceous vegetation since >2000 years ago, until recent decades when all cores document a consistent, abrupt transition in vegetation composition toward a present-day dominance of dry-adapted *Sphagnum* mosses (*S.* sect. *Sphagnum* and *S.* sect. *Acutifolia*) and an increased abundance of shrubs, both indicating a dry ombrotrophic (rain-fed) bog environment (Figs. 2 and A1–A6). It is noted that this transition in
430   core TQ22-C6 appears slightly more complex: *Sphagnum* mosses were present somewhat earlier (median age 1838 CE) and had undergone both abundance fluctuations and species turnovers, but the vegetation composition similar to that in other cores was eventually established in recent decades (Fig. A6). Principal component analysis of the full macrofossil dataset further reveals that the recent abrupt transition to bog-like vegetation was preceded by a longer-term slow shift in the same direction since the LIA (Fig. 4b).

435   While a previous study at the same site has already documented this abrupt transition in vegetation composition, which specifically occurred at about 1895 CE based on the analysis of a single peat core (TQ16; Fig. 1c) (Liu et al., 2024b), our new data from multiple cores make a strong case that this is a site-wide phenomenon of fen-bog transition (FBT) with clear signs of regime-shift behavior, i.e., gradual changes followed by sudden shifts (Scheffer and Carpenter, 2003; Loisel and Yu, 2013; Loisel and Bunsen, 2020).

440   Instrumental climate data from northern Northeast China indicate a temperature increase of by up to 4°C since the end of the nineteenth century (Zhang et al., 2011; Yao et al., 2021). The recent FBT at our site underscores the high sensitivity of ecosystem structures in such young, shallow, and permafrost-underlain peatlands to rapid and large-magnitude climate warming. Loisel and Yu (2013) previously described a conceptual model of "warming-driven FBT" for non-permafrost peatlands to explain how anthropogenic climate warming facilitates *Sphagnum* moss establishment and
445   oligotrophication through surface drying and ecohydrological feedback. For permafrost peatlands, however, we anticipate that the additional permafrost–hydrology feedback further reinforces the processes underlying this model: deepening active

layers—the first-stage response to warming-driven permafrost degradation (Swindles et al., 2015; Hugelius et al., 2020)—would further draw down water tables to enhance surface drying. This is supported by our *Sphagnum* $\delta^{13}C_{cell}$ data, which show very low values (corrected values less than –30‰) when *Sphagnum* mosses initially replaced herbaceous vegetation in macrofossil records (Fig. 6b), indicating extremely dry conditions when FBT occurred (see following Section 4.3 on interpretations of *Sphagnum* $\delta^{13}C_{cell}$ data). Several other studies have documented recent FBT or *Sphagnum* moss expansion in permafrost peatlands elsewhere (Magnan et al., 2018; Taylor et al., 2019; Magnan et al., 2022; Chartrand et al., 2023; Piilo et al., 2023), likely driven by mechanisms similar to that in our record.

There is extensive literature describing the highly dynamic and heterogenous nature of permafrost peatlands with complex ecosystem shifts in response to natural climate variability (Zoltai, 1993; Jones et al., 2013; Gao and Couwenberg, 2015; Treat et al., 2016; Zhang et al., 2018b; Sim et al., 2021; Piilo et al., 2023; Xia et al., 2024a). Specifically, climated-riven permafrost aggradation and degradation can strongly alter surface morphology, forming palsas, peat plateaus, thermokarst collapses, fen-bog complexes, and lakes/ponds, with each following different succession pathways (Olefeldt et al., 2021). However, Tuqiang peatland is a site showing historical stability, along with homogeneity in recent ecosystem shifts and present-day structure free of relict permafrost landforms (Fig. 1d). We attribute such major differences to the low ice content of regional permafrost compared to previous studies conducted in Europe and North America (Brown et al., 1997; Jin et al., 2016; Olefeldt et al., 2016). Again, our study region is outside the circumpolar thermokarst landscape (Olefeldt et al., 2021).

The ongoing climate warming, active layer deepening, and, in particular, the recent transition to the dominance of *Sphagnum* mosses may collectively alter the balance between plant productivity and OM decomposition, with profound consequences for the peatland C sink function (Clymo and Hayward, 1982; van Breemen, 1995; Loisel and Yu, 2013). Some studies have attempted to interpret time series of depth-specific aCAR to understand the temporal shifts in the rate of C sink (Swindles et al., 2015; Zhang et al., 2018a; Zhang et al., 2020a; Sim et al., 2021; Cleary et al., 2024), but direct comparisons between recent and long-term rates can be questioned (Young et al., 2019). Here, we found that the present-day NECB, estimated over two monitored years (Guo et al., 2018; Sun et al., 2024), is much higher than the centuries- and millennia-averaged NECB, estimated from long-term aCAR across entire peat core columns (Fig. 5). This suggests a potential stronger C sink capacity under present conditions compared to the past. However, we caution that the present-day NECB is likely an overestimate, due to the short measurement period not accounting for low-frequency disturbances (e.g., wildfire) and the inconsistent methodology (C fluxes are estimated using the concentration gradient method in freezing winter) (Miao et al., 2012b; Sun et al., 2024).

At our site, *Sphagnum* peat accumulation is quite rapid, reaching a thickness of about 40 cm material over several decades (Fig. 2). Peat accumulation modeling quantifies near-surface peat buildup as being governed by a stable and rapid input of plant litter and a stable and rapid proportional decay, with possible recalcitrance in recently formed OM (Fig. 3). Therefore, the present-day stronger C sink is likely primarily related to the persistent surficial peat accumulation from *Sphagnum* litter, which must greatly outweigh any deep C loss caused by deeper active layers and aerobic conditions.

Together, our analysis suggests that anthropogenic warming-driven FBT is likely amplified by permafrost–hydrology feedback, with no sign of a reduction in the C sink. In order to understand possible mechanisms for the persistence of C sink function, we next investigate the pattern of recent environmental changes documented in isotopic ratios of *Sphagnum* macrofossils.

4.3 Progressively wetter conditions over the last several decades

Isotopic records from *Sphagnum* macrofossils offer further insights into changes in surface conditions since *Sphagnum* mosses became dominant at our site, providing essential context for understanding ongoing environmental trajectories and their drivers. *Sphagnum* $\delta^{13}C_{cell}$ is a proxy for surface wetness based on the "water film" mechanism, which has been well established through multiple studies (Rice and Giles, 1996; Williams and Flanagan, 1996; Loisel et al., 2009; Xia et al., 2020). Briefly, higher $\delta^{13}C_{cell}$ values indicate wetter conditions, as a thicker water film on leaf surfaces reduces isotopic fractionation caused by carboxylation (Farquhar et al., 1989). For peatlands like ours relying on precipitation as the primary source of water, *Sphagnum* $\delta^{18}O_{cell}$ is a proxy for precipitation $\delta^{18}O$ (Daley et al., 2010; Granath et al., 2018; Xia et al., 2018), which is controlled by multiple atmospheric drivers such as temperature, precipitation amount or seasonality, and moisture sources (Dansgaard, 1964).

The $\delta^{13}C_{cell}$ records indicate that the peatland has undergone gradual trends, lacking fluctuations and being asynchronous among different cores, from very dry to wetter conditions over the last several decades (Fig. 6b). Such pattern of moisture changes cannot be simply attributed to a common driver of precipitation, which exhibits large inter-annual variability (Fig. 6a). By contrast, the $\delta^{18}O_{cell}$ records show no long-term trend but instead contain large sample-to-sample fluctuations (Fig. 6c), coinciding with the pronounced inter-annual atmospheric variability that may affect precipitation $\delta^{18}O$ (Fig. 6a, d). Therefore, our *Sphagnum* $\delta^{13}C_{cell}$ and $\delta^{18}O_{cell}$ records present two seemingly conflicting phenomena: evidence for the rain-fed nature of *Sphagnum* moss habitats yet no direct effects on their wetness. Here, we interpret these data as indicating that *Sphagnum* wetness is controlled by internal, locally paced surface processes independent of the peatland water balance's response to external climate forcing. As described below, we specifically hypothesize that such internal dynamics can be attributed to gradual subsidence from the degradation of ice-poor permafrost or the ecohydrological feedback driven by the ecosystem engineer *Sphagnum* mosses.

Previous studies have proposed an empirical stage model predicting that active layer deepening and surface drying in permafrost peatlands would be succeeded by ground collapse, thermokarst formation, and land surface wetting once thaw progresses into ice-rich layers (Swindles et al., 2015; Hugelius et al., 2020). A newly published global synthesis of peatland water table reconstructions also revealed that those permafrost peatlands showing an ongoing wetting trend had experienced drier "pre-conditions" before the wet shifts (Sim et al., 2021; Zhang et al., 2022). Therefore, the shift from dry to wet conditions over the last several decades documented in our records appears to be an expected outcome for peatlands under warming-driven permafrost degradation. However, field observations at Tuqiang peatland show no sign of peat shrinkage, cracking, or collapse—features that characterize the wetting stage (Fig. 1d). Therefore, unlike the empirical stage model

developed for ice-rich peatlands in Europe and North America, we hypothesize that the wetting may be linked to surface
515   subsidence resulting from a combination of gradual thaw and decomposition-induced peat loss, which raised the water table
when the effect of active layer deepening slowed down. For simplicity, we term this general mechanism as surface
adjustment–hydrology feedback (Waddington et al., 2015).

Sphagnum mosses are well-known ecosystem engineers that possess multiple plant properties to modify local
environmental conditions in ways that favor their success and peat formation (Clymo and Hayward, 1982; van Breemen,
520   1995; Rydin and Jeglum, 2013). Among these properties, they have an extraordinary water-holding capacity, typically
containing several to tens of times more water than their tissue weight within their hyaline cells and external pore spaces,
and can maintain a capillary fringe to distribute water under various conditions (Clymo and Hayward, 1982; Rydin and
Jeglum, 2013). Additionally, *Sphagnum* peat is a poor heat conductor, and as an insulating layer, it may further contribute to
slowing down active layer deepening (van Breemen, 1995; Park et al., 2018). Therefore, we hypothesize that the wetting
525   may also result from plant-mediated ecohydrological feedback (vegetation–hydrology feedback) regulating local moisture
dynamics as *Sphagnum* peat gradually built up.

Overall, the isotopic records document internally driven, progressively wetter conditions at Tuqiang peatland in
recent decades, indicating that anthropogenic climate warming and concurrent permafrost degradation would not lead to
complete desiccation (runaway drying scenario). Regardless of the actual mechanisms, the peatland demonstrates resilience
530   in mitigating drying. In addition to warming-induced increases in plant productivity (Gallego-Sala et al., 2018), the input of
recalcitrant and fire-resistant *Sphagnum* litter (Loisel and Yu, 2013), and increased acidity inhibiting microbial activity (van
Breemen, 1995), surface wetting may contribute to maintaining or even enhancing the C sink and might be related to the
high NECB observed in atmospheric C flux measurements (Fig. 5).

5 Synthesis and conclusions

535   Through a detailed multi-core and multi-proxy anatomy of a typical ice-poor permafrost peatland in eastern Eurasia,
we are able to understand how peatland formation, succession, and surface conditions responded to long-term climate
variability and identify the roles of permafrost dynamics in regulating these responses. We summarize the main findings as a
conceptual diagram describing the evolution of young, shallow, and ice-poor permafrost peatlands under climate change and
into the future (Fig. 8). The general conclusions and broad implications are as follows:

540   (1) Permafrost aggradation over permeable mineral-rich soils or substrates is a potentially important but overlooked agent in
the formation of new peatland areas by maintaining poorly drained, waterlogged conditions. This permafrost–hydrology
feedback highlights the need to consider surficial geology and cryosphere dynamics in understanding the genesis of
global peatlands.

(2) Ice-poor permafrost peatlands exhibit weak sensitivity to natural climate variability but clear regime-shift behavior
545   under rapid and large-magnitude anthropogenic climate warming. Unlike ice-rich permafrost peatlands with highly

dynamic surface morphology, ice-poor permafrost peatlands are characterized by a high degree of stability and homogeneity. The simple succession without involving thermokarst collapse means that their future greenhouse gas emissions and radiative forcing should be substantially smaller than that predicted by models developed for ice-rich permafrost peatlands (Hugelius et al., 2020).

550   (3) Several internal feedback mechanisms may be involved in maintaining the hydrology and C accumulation of ice-poor permafrost peatlands under ongoing climate change. These behaviors reflect peatlands functioning as complex adaptive systems (Belyea and Baird, 2006).

    (4) Our analysis combining present-day atmospheric C flux measurements presents empirical evidence that similar ice-poor permafrost peatlands in eastern Eurasia are persistent C sinks. Simple protection measures such as fire prevention

555   programs currently being implemented in northern Northeast China are effective in preserving these significant terrestrial C stocks in the future.
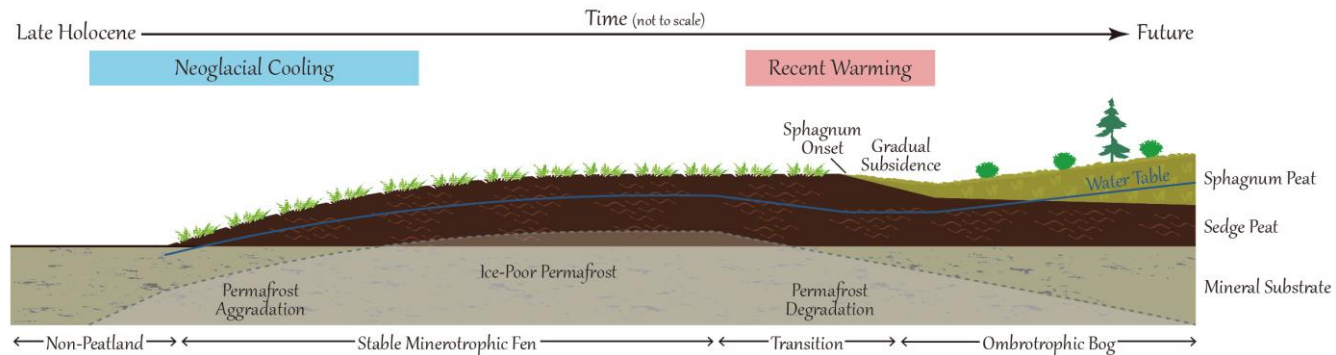
Figure 8. A conceptual diagram for the evolution of young, shallow, and ice-poor permafrost peatlands under climate

560   change based on findings of this study.

Appendix A: Macrofossil diagram of peatland cores
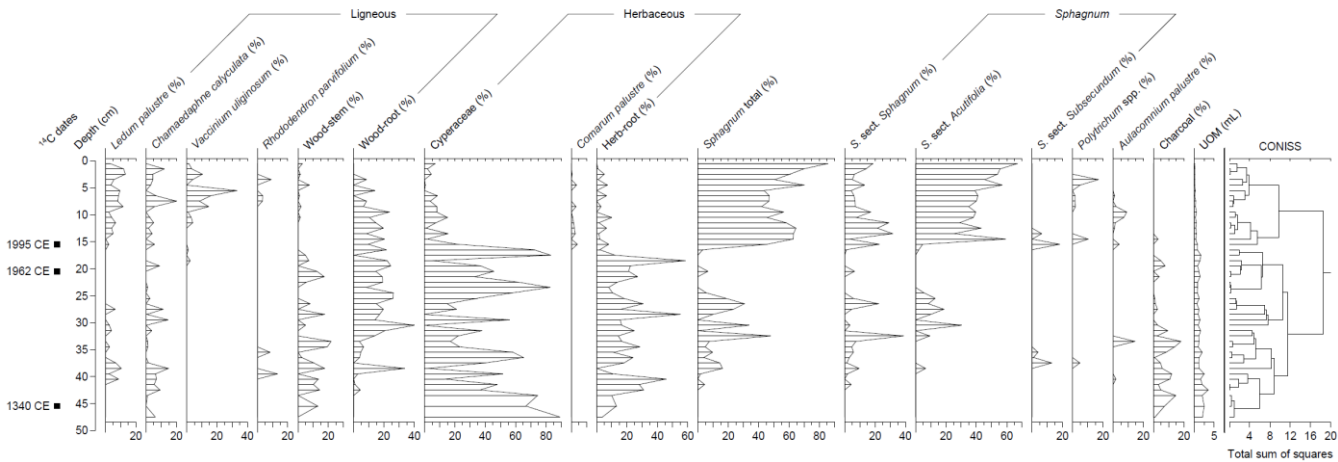
Figure A1. Macrofossil diagram of core TQ22-C1.

565
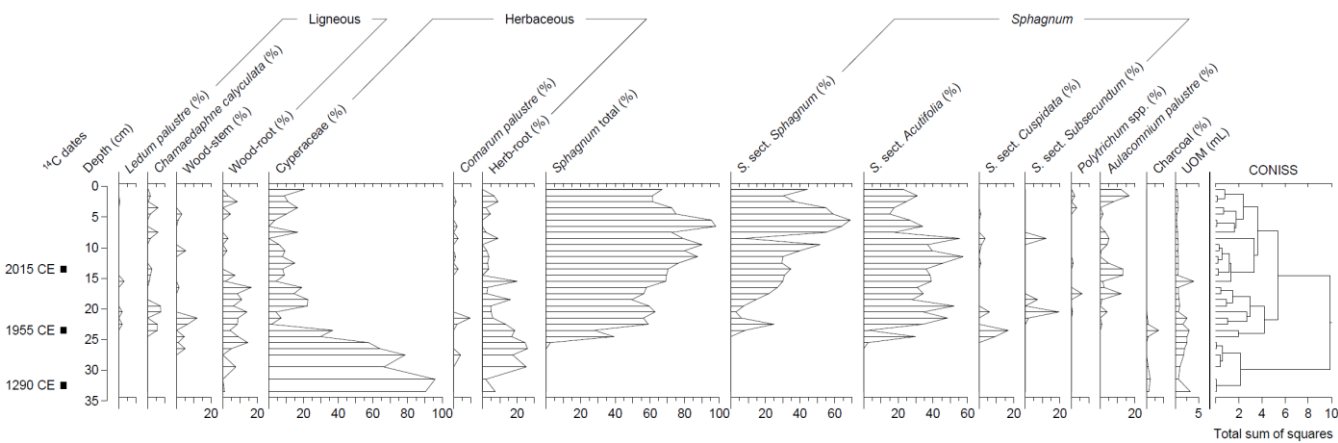
Figure A2. Macrofossil diagram of core TQ22-C2.
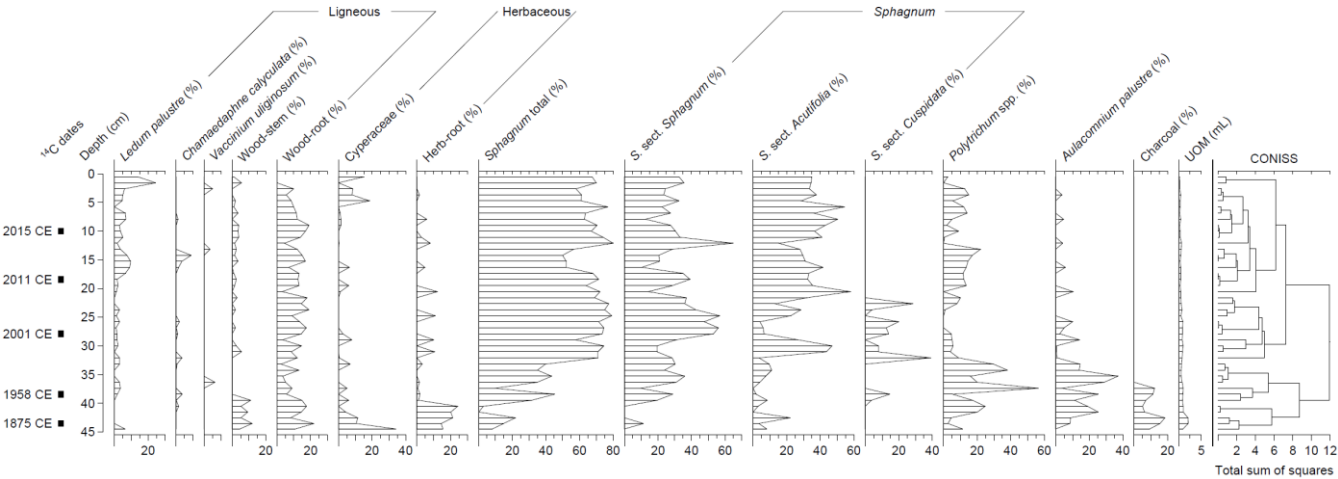
Figure A3. Macrofossil diagram of core TQ22-C3.
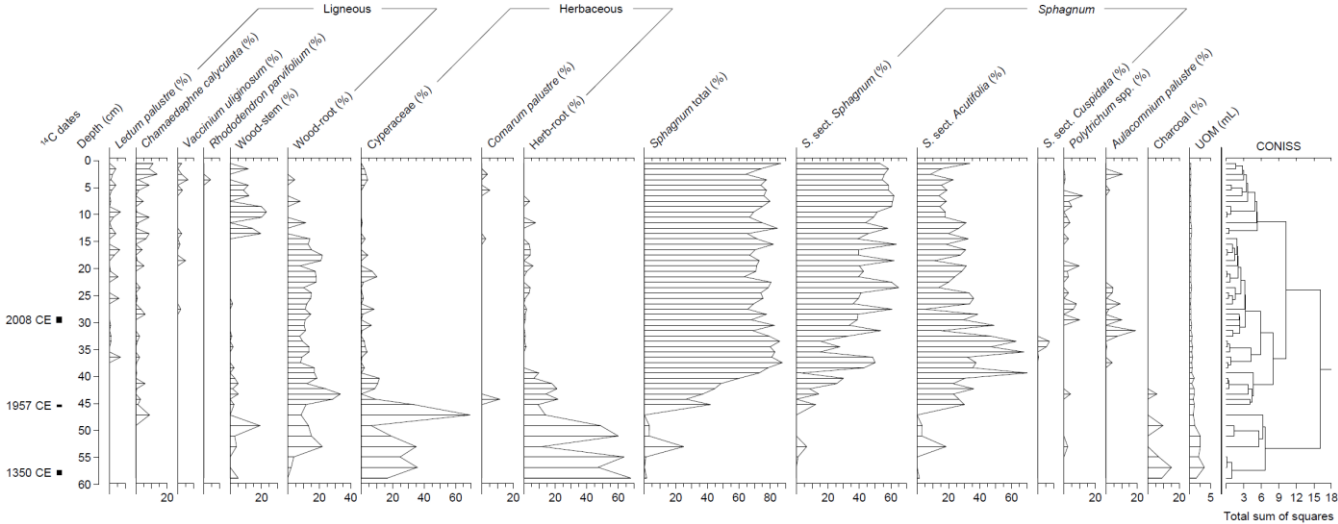
Figure A4. Macrofossil diagram of core TQ22-C4.

575
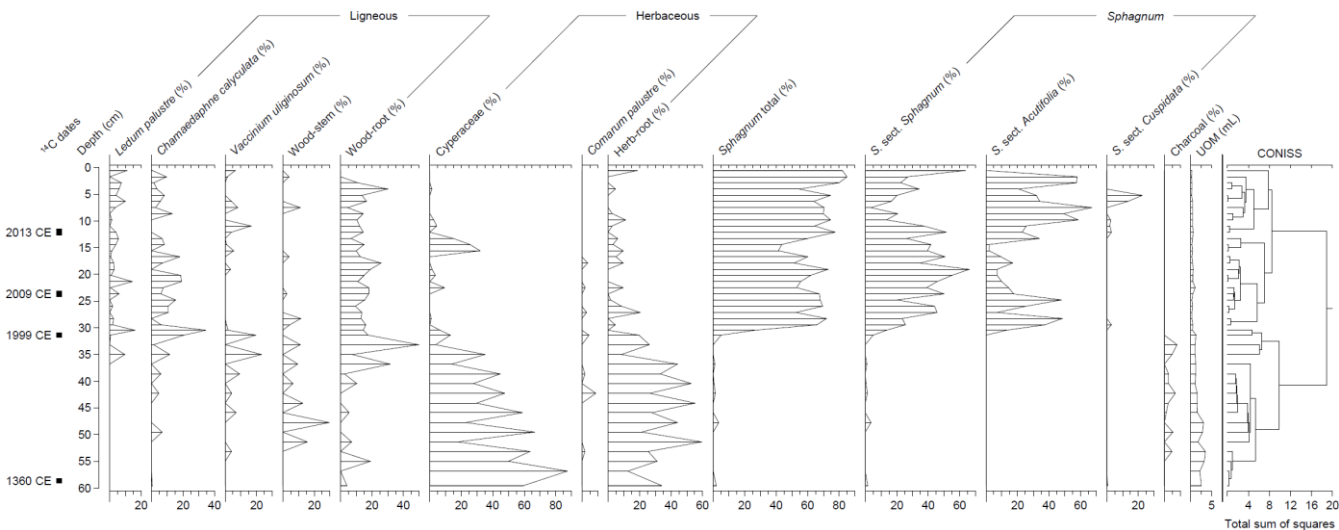
Figure A5. Macrofossil diagram of core TQ22-C5.
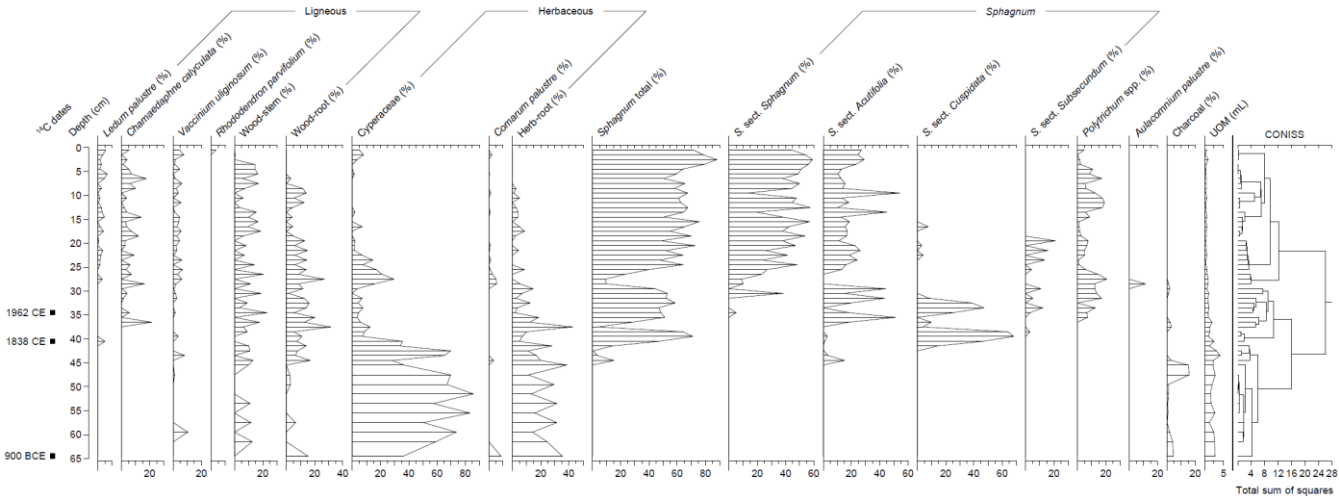
Figure A6. Macrofossil diagram of core TQ22-C6.

580

Data availability. The data presented in this study are available on request from the corresponding author.

Author contribution. ZY and ZX designed and supervised the study. ZX and FC conducted the field work. FC, MG, and ZX
conducted the laboratory work. ZX, FC, and ZY contributed to the data interpretations. ZX and FC wrote the manuscript. ZY
585   edited the manuscript.

Competing interests. The authors declare that they have no conflict of interest.

Acknowledgements. We thank Tingwan Yang, Wei Yang, and Shuai Zhang for fieldwork assistance, Yanmin Dong for
590   radiocarbon measurements, and Camille Risi for providing LMDZ4 output.

Financial support. This work was supported by the National Natural Science Foundation of China (42330509, 42494822, 42201167), Fundamental Research Funds for the Central Universities (2412023YQ006, 135112004), and Natural Science Foundation of Jilin Province (20230101077JC).

595   **References**

Bao, K.-s., Shen, J., Zhang, Y., Wang, J., and Wang, G.-p.: A 200-year record of polycyclic aromatic hydrocarbons contamination in an ombrotrophic peatland in Great Hinggan Mountain, northeast China, J. Mountain Sci., 11, 1085–1096, https://doi.org/10.1007/s11629-014-3167-1, 2014

Bao, K., Xing, W., Yu, X., Zhao, H., McLaughlin, N., Lu, X., and Wang, G.: Recent atmospheric dust deposition in an
600   ombrotrophic peat bog in Great Hinggan Mountain, Northeast China, Sci. Total Environ., 431, 33–45, https://doi.org/10.1016/j.scitotenv.2012.05.014, 2012

Bauer, I. E. and Vitt, D. H.: Peatland dynamics in a complex landscape: Development of a fen-bog complex in the Sporadic Discontinuous Permafrost zone of northern Alberta, Canada, Boreas, 40, 714–726, https://doi.org/10.1111/j.1502-3885.2011.00210.x, 2011

605   Belyea, L. R. and Baird, A. J.: Beyond "the limits to peat bog growth": Cross-scale feedback in peatland development, Ecological Monographs, 76, 299–322, https://doi.org/10.1890/0012-9615(2006)076[0299:BTLTPB]2.0.CO;2, 2006

Borge, A. F., Westermann, S., Solheim, I., and Etzelmüller, B.: Strong degradation of palsas and peat plateaus in northern Norway during the last 60 years, Cryosphere, 11, 1–16, https://doi.org/10.5194/tc-11-1-2017, 2017

Brown, J., Ferrians Jr, O. J., Heginbottom, J. A., and Melnikov, E. S.: Circum-Arctic map of permafrost and ground-ice
610   conditions, Report 45, https://doi.org/10.3133/cp45, 1997.

Camill, P. and Clark, J. S.: Climate change disequilibrium of boreal permafrost peatlands caused by local processes, Am. Nat., 151, 207–222, http://doi.org/10.1086/286112, 1998

Camill, P., Barry, A., Williams, E., Andreassi, C., Limmer, J., and Solick, D.: Climate-vegetation-fire interactions and their impact on long-term carbon dynamics in a boreal peatland landscape in northern Manitoba, Canada, J. Geophys. Res., 114,
615   G04017, https://doi.org/10.1029/2009JG001071, 2009

Charman, D. J., Beilman, D. W., Blaauw, M., Booth, R. K., Brewer, S., Chambers, F. M., Christen, J. A., Gallego-Sala, A., Harrison, S. P., Hughes, P. D. M., Jackson, S. T., Korhola, A., Mauquoy, D., Mitchell, F. J. G., Prentice, I. C., van der Linden, M., De Vleeschouwer, F., Yu, Z. C., Alm, J., Bauer, I. E., Corish, Y. M. C., Garneau, M., Hohl, V., Huang, Y., Karofeld, E., Le Roux, G., Loisel, J., Moschen, R., Nichols, J. E., Nieminen, T. M., MacDonald, G. M., Phadtare, N. R.,

620 Rausch, N., Sillasoo, Ü., Swindles, G. T., Tuittila, E. S., Ukonmaanaho, L., Väliranta, M., van Bellen, S., van Geel, B., Vitt, D. H., and Zhao, Y.: Climate-related changes in peatland carbon accumulation during the last millennium, Biogeosciences, 10, 929–944, https://doi.org/10.5194/bg-10-929-2013, 2013

Chartrand, P. G., Sonnentag, O., Sanderson, N. K., and Garneau, M.: Recent peat and carbon accumulation on changing permafrost landforms along the Mackenzie River valley, Northwest Territories, Canada, Environ. Res. Lett., 18, 095002, 625 http://doi.org/10.1088/1748-9326/ace9ed, 2023

Cleary, K. G., Xia, Z., and Yu, Z.: The growth and carbon sink of tundra peat patches in Arctic Alaska, J. Geophys. Res. Biogeosci., 129, e2023JG007890, https://doi.org/10.1029/2023JG007890, 2024

Clymo, R. S.: The limits of peat bog growth, Philos. Trans. R. Soc. B, 303, 368–388, https://doi.org/10.1098/rstb.1984.0002, 1984

630 Clymo, R. S. and Hayward, P. M.: The Ecology of *Sphagnum*, in: Bryophyte Ecology, edited by: Smith, A. J. E., Springer Netherlands, Dordrecht, Netherlands, 229–289, https://doi.org/10.1007/978-94-009-5891-3_8, 1982.

Clymo, R. S., Turunen, J., and Tolonen, K.: Carbon accumulation in peatland, Oikos, 81, 368–388, https://doi.org/10.2307/3547057, 1998

Cooper, M. D. A., Estop-Aragonés, C., Fisher, J. P., Thierry, A., Garnett, M. H., Charman, D. J., Murton, J. B., Phoenix, G. 635 K., Treharne, R., Kokelj, S. V., Wolfe, S. A., Lewkowicz, A. G., Williams, M., and Hartley, I. P.: Limited contribution of permafrost carbon to methane release from thawing peatlands, Nat. Clim. Change, 7, 507–511, https://doi.org/10.1038/nclimate3328, 2017

Daley, T. J., Barber, K. E., Street-Perrott, F. A., Loader, N. J., Marshall, J. D., Crowley, S. F., and Fisher, E. H.: Holocene climate variability revealed by oxygen isotope analysis of *Sphagnum* cellulose from Walton Moss, northern England, Quat. 640 Sci. Rev., 29, 1590–1601, https://doi.org/10.1016/j.quascirev.2009.09.017, 2010

Dansgaard, W.: Stable isotopes in precipitation, Tellus, 16, 436–468, https://doi.org/10.3402/tellusa.v16i4.8993, 1964

Debolskiy, M. V., Alexeev, V. A., Hock, R., Lammers, R. B., Shiklomanov, A., Schulla, J., Nicolsky, D., Romanovsky, V. E., and Prusevich, A.: Water balance response of permafrost-affected watersheds to changes in air temperatures, Environ. Res. Lett., 16, 084054, https://doi.org/10.1088/1748-9326/ac12f3, 2021

645 Errington, R. C., Macdonald, S. E., and Bhatti, J. S.: Rate of permafrost thaw and associated plant community dynamics in peatlands of northwestern Canada, J. Ecol., 112, 1565–1582, https://doi.org/10.1111/1365-2745.14339, 2024

Estop-Aragonés, C., Cooper, M. D. A., Fisher, J. P., Thierry, A., Garnett, M. H., Charman, D. J., Murton, J. B., Phoenix, G. K., Treharne, R., Sanderson, N. K., Burn, C. R., Kokelj, S. V., Wolfe, S. A., Lewkowicz, A. G., Williams, M., and Hartley, I. P.: Limited release of previously-frozen C and increased new peat formation after thaw in permafrost peatlands, Soil Biol. 650 Biochem., 118, 115–129, https://doi.org/10.1016/j.soilbio.2017.12.010, 2018

Farquhar, G. D., Ehleringer, J. R., and Hubick, K. T.: Carbon isotope discrimination and photosynthesis, Annu. Rev. Plant Physiol. Plant Mol. Biol., 40, 503–537, https://doi.org/10.1146/annurev.pp.40.060189.002443, 1989

Fewster, R. E., Morris, P. J., Ivanovic, R. F., Swindles, G. T., Peregon, A. M., and Smith, C. J.: Imminent loss of climate space for permafrost peatlands in Europe and Western Siberia, Nat. Clim. Change, 12, 373–379, 655 https://doi.org/10.1038/s41558-022-01296-7, 2022

Fewster, R. E., Morris, P. J., Swindles, G. T., Ivanovic, R. F., Treat, C. C., and Jones, M. C.: Holocene vegetation dynamics of circum-Arctic permafrost peatlands, Quat. Sci. Rev., 307, 108055, https://doi.org/10.1016/j.quascirev.2023.108055, 2023

Frey, K. E. and Smith, L. C.: Amplified carbon release from vast West Siberian peatlands by 2100, Geophys. Res. Lett., 32, L09401, https://doi.org/10.1029/2004GL022025, 2005

660 Gałka, M., Szal, M., Watson, E. J., Gallego-Sala, A., Amesbury, M. J., Charman, D. J., Roland, T. P., Edward Turner, T., and Swindles, G. T.: Vegetation succession, carbon accumulation and hydrological change in subarctic peatlands, Abisko, northern Sweden, Permafr. Periglac. Process., 28, 589–604, https://doi.org/10.1002/ppp.1945, 2017

Gallego-Sala, A. V., Charman, D. J., Brewer, S., Page, S. E., Prentice, I. C., Friedlingstein, P., Moreton, S., Amesbury, M. J., Beilman, D. W., Björck, S., Blyakharchuk, T., Bochicchio, C., Booth, R. K., Bunbury, J., Camill, P., Carless, D., Chimner, R.
665 A., Clifford, M., Cressey, E., Courtney-Mustaphi, C., De Vleeschouwer, F., de Jong, R., Fialkiewicz-Koziel, B., Finkelstein, S. A., Garneau, M., Githumbi, E., Hribjlan, J., Holmquist, J., Hughes, P. D. M., Jones, C., Jones, M. C., Karofeld, E., Klein, E. S., Kokfelt, U., Korhola, A., Lacourse, T., Le Roux, G., Lamentowicz, M., Large, D., Lavoie, M., Loisel, J., Mackay, H., MacDonald, G. M., Makila, M., Magnan, G., Marchant, R., Marcisz, K., Martínez Cortizas, A., Massa, C., Mathijssen, P., Mauquoy, D., Mighall, T., Mitchell, F. J. G., Moss, P., Nichols, J., Oksanen, P. O., Orme, L., Packalen, M. S., Robinson, S.,
670 Roland, T. P., Sanderson, N. K., Sannel, A. B. K., Silva-Sánchez, N., Steinberg, N., Swindles, G. T., Turner, T. E., Uglow, J., Väliranta, M., van Bellen, S., van der Linden, M., van Geel, B., Wang, G., Yu, Z., Zaragoza-Castells, J., and Zhao, Y.: Latitudinal limits to the predicted increase of the peatland carbon sink with warming, Nat. Clim. Change, 8, 907–913, https://doi.org/10.1038/s41558-018-0271-1, 2018

Gao, C., He, J., Zhang, Y., Cong, J., Han, D., and Wang, G.: Fire history and climate characteristics during the last
675 millennium of the Great Hinggan Mountains at the monsoon margin in northeastern China, Glob. Planet. Change, 162, 313–320, https://doi.org/10.1016/j.gloplacha.2018.01.021, 2018

Gao, Y. and Couwenberg, J.: Carbon accumulation in a permafrost polygon peatland: Steady long-term rates in spite of shifts between dry and wet conditions, Global Change Biol., 21, 803–815, https://doi.org/10.1111/gcb.12742, 2015

Ge, Q., Zheng, J., Hao, Z., and Liu, H.: General characteristics of climate changes during the past 2000 years in China, Sci.
680 China Earth Sci., 56, 321–329, https://doi.org/10.1007/s11430-012-4370-y, 2013

Gorham, E.: Northern peatlands: Role in the carbon cycle and probable responses to climatic warming, Ecol. Appl., 1, 182–195, https://doi.org/10.2307/1941811, 1991

Granath, G., Rydin, H., Baltzer, J. L., Bengtsson, F., Boncek, N., Bragazza, L., Bu, Z. J., Caporn, S. J. M., Dorrepaal, E., Galanina, O., Gałka, M., Ganeva, A., Gillikin, D. P., Goia, I., Goncharova, N., Hájek, M., Haraguchi, A., Harris, L. I.,
685 Humphreys, E., Jiroušek, M., Kajukało, K., Karofeld, E., Koronatova, N. G., Kosykh, N. P., Lamentowicz, M., Lapshina, E., Limpens, J., Linkosalmi, M., Ma, J. Z., Mauritz, M., Munir, T. M., Natali, S. M., Natcheva, R., Noskova, M., Payne, R. J., Pilkington, K., Robinson, S., Robroek, B. J. M., Rochefort, L., Singer, D., Stenøien, H. K., Tuittila, E. S., Vellak, K., Verheyden, A., Waddington, J. M., and Rice, S. K.: Environmental and taxonomic controls of carbon and oxygen stable isotope composition in *Sphagnum* across broad climatic and geographic ranges, Biogeosciences, 15, 5189–5202,
690 https://doi.org/10.5194/bg-15-5189-2018, 2018

Guo, Y., Song, C., Tan, W., Wang, X., and Lu, Y.: Hydrological processes and permafrost regulate magnitude, source and chemical characteristics of dissolved organic carbon export in a peatland catchment of northeastern China, Hydrol. Earth Syst. Sci., 22, 1081–1093, https://doi.org/10.5194/hess-22-1081-2018, 2018

Han, D., Gao, C., Yu, Z., Yu, X., Li, Y., Cong, J., and Wang, G.: Late Holocene vegetation and climate changes in the Great
695 Hinggan Mountains, northeast China, Quat. Int., 532, 138–145, https://doi.org/10.1016/j.quaint.2019.11.017, 2019

Harris, L. I., Olefeldt, D., Pelletier, N., Blodau, C., Knorr, K.-H., Talbot, J., Heffernan, L., and Turetsky, M.: Permafrost thaw causes large carbon loss in boreal peatlands while changes to peat quality are limited, Global Change Biol., 29, 5720–5735, https://doi.org/10.1111/gcb.16894, 2023

Heffernan, L., Estop-Aragonés, C., Knorr, K.-H., Talbot, J., and Olefeldt, D.: Long-term impacts of permafrost thaw on carbon storage in peatlands: Deep losses offset by surficial accumulation, J. Geophys. Res. Biogeosci., 125, e2019JG005501, https://doi.org/10.1029/2019JG005501, 2020

Heffernan, L., Estop-Aragonés, C., Kuhn, M. A., Holger-Knorr, K., and Olefeldt, D.: Changing climatic controls on the greenhouse gas balance of thermokarst bogs during succession after permafrost thaw, Global Change Biol., 30, e17388, https://doi.org/10.1111/gcb.17388, 2024

Hodgkins, S. B., Tfaily, M. M., McCalley, C. K., Logan, T. A., Crill, P. M., Saleska, S. R., Rich, V. I., and Chanton, J. P.: Changes in peat chemistry associated with permafrost thaw increase greenhouse gas production, Proc. Natl. Acad. Sci. USA, 111, 5819–5824, https://doi.org/10.1073/pnas.1314641111, 2014

Hugelius, G., Loisel, J., Chadburn, S., Jackson, R. B., Jones, M., MacDonald, G., Marushchak, M., Olefeldt, D., Packalen, M., Siewert, M. B., Treat, C., Turetsky, M., Voigt, C., and Yu, Z.: Large stocks of peatland carbon and nitrogen are vulnerable to permafrost thaw, Proc. Natl. Acad. Sci. USA, 117, 20438–20446, https://doi.org/10.1073/pnas.1916387117, 2020

Hughes, P. D. M. and Barber, K. E.: Contrasting pathways to ombrotrophy in three raised bogs from Ireland and Cumbria, England, Holocene, 14, 65–77, https://doi.org/10.1191/0959683604hl690rp, 2004

Hunt, S., Yu, Z., and Jones, M.: Lateglacial and Holocene climate, disturbance and permafrost peatland dynamics on the Seward Peninsula, western Alaska, Quat. Sci. Rev., 63, 42–58, https://doi.org/10.1016/j.quascirev.2012.11.019, 2013

Ishikawa, M., Sharkhuu, N., Zhang, Y., Kadota, T., and Ohata, T.: Ground thermal and moisture conditions at the southern boundary of discontinuous permafrost, Mongolia, Permafr. Periglac. Process., 16, 209–216, https://doi.org/10.1002/ppp.483, 2005

Jiang, J., Meng, B., Wang, H., Liu, H., Song, M., He, Y., Zhao, C., Cheng, J., Chu, G., Krivonogov, S., Liu, W., and Liu, Z.: Spatial patterns of Holocene temperature changes over mid-latitude Eurasia, Nat. Commun., 15, 1507, https://doi.org/10.1038/s41467-024-45883-y, 2024

Jin, H.-J., Chang, X.-L., Luo, D.-L., He, R.-X., Lü, L.-Z., Yang, S.-Z., Guo, D.-X., Chen, X.-M., and Harris, S. A.: Evolution of permafrost in Northeast China since the Late Pleistocene, Sciences in Cold and Arid Regions, 8, 269–296, 2016

Jin, H., Li, S., Cheng, G., Shaoling, W., and Li, X.: Permafrost and climatic change in China, Glob. Planet. Change, 26, 387–404, https://doi.org/10.1016/S0921-8181(00)00051-5, 2000

Jones, M. C., Booth, R. K., Yu, Z., and Ferry, P.: A 2200-year record of permafrost dynamics and carbon cycling in a collapse-scar bog, interior Alaska, Ecosystems, 16, 1–19, https://doi.org/10.1007/s10021-012-9592-5, 2013

Jones, M. C., Harden, J., O'Donnell, J., Manies, K., Jorgenson, T., Treat, C., and Ewing, S.: Rapid carbon loss and slow recovery following permafrost thaw in boreal peatlands, Global Change Biol., 23, 1109–1127, https://doi.org/10.1111/gcb.13403, 2017

Kaislahti Tillman, P., Holzkämper, S., Kuhry, P., Sannel, A. B. K., Loader, N. J., and Robertson, I.: Stable carbon and oxygen isotopes in *Sphagnum fuscum* peat from subarctic Canada: Implications for palaeoclimate studies, Chem. Geol., 270, 216–226, https://doi.org/10.1016/j.chemgeo.2009.12.001, 2010

Knoblauch, C., Beer, C., Liebner, S., Grigoriev, M. N., and Pfeiffer, E.-M.: Methane production as key to the greenhouse gas budget of thawing permafrost, Nat. Clim. Change, 8, 309–312, https://doi.org/10.1038/s41558-018-0095-z, 2018

Korhola, A., Ruppel, M., Seppä, H., Väliranta, M., Virtanen, T., and Weckström, J.: The importance of northern peatland expansion to the late-Holocene rise of atmospheric methane, Quat. Sci. Rev., 29, 611–617, https://doi.org/10.1016/j.quascirev.2009.12.010, 2010

Leuenberger, M.: To what extent can ice core data contribute to the understanding of plant ecological developments of the past?, in: Stable Isotopes as Indicators of Ecological Change, edited by: Dawson, T. E., and Siegwolf, R. T. W., Elsevier, 211–233, https://doi.org/10.1016/S1936-7961(07)01014-7, 2007.

Li, X., Zhao, C., and Zhou, X.: Vegetation pattern of Northeast China during the special periods since the Last Glacial Maximum, Sci. China Earth Sci., 62, 1224–1240, https://doi.org/10.1007/s11430-018-9347-3, 2019

Liu, C., Yue, H., Zhang, W., Yao, Z., Pan, Y., Wang, X., Song, C., Butterbach-Bahl, K., and Dannenmann, M.: Alder expansion stimulates nitrogen oxide (NO_x) emissions from southern Eurasian permafrost peatlands, Global Change Biol., 30, e17368, https://doi.org/10.1111/gcb.17368, 2024a

Liu, H., Han, D., and Wang, G.: Considering the autogenic processes of the ecosystem to analyze the sensitivity of peatland carbon accumulation to temperature and hydroclimate change, Catena, 236, 107717, https://doi.org/10.1016/j.catena.2023.107717, 2024b

Liu, H., Yu, Z., Han, D., Gao, C., Yu, X., and Wang, G.: Temperature influence on peatland carbon accumulation over the last century in Northeast China, Clim. Dyn., 53, 2161–2173, https://doi.org/10.1007/s00382-019-04813-1, 2019a

Liu, J., Liu, Q., Wu, J., Chu, G., and Liu, J.: *N*-alkanes distributions and compound-specific carbon isotope records and their paleoenviromental significance of sediments from Lake Sifangshan in the Great Khingan Mountain, Northeastern China, Journal of Lake Sciences, 29, 498–511, 2017 (in Chinese with an English abstract).

Liu, X., Zhan, T., Zhou, X., Wu, H., Li, Q., Zhao, C., Qiao, Y., Jiang, S., Tu, L., Ma, Y., Zhang, J., Jiang, X., Lou, B., Zhang, X., and Zhou, X.: Late onset of the Holocene rainfall maximum in northeastern China inferred from a pollen record from the sediments of Tianchi Crater Lake, Quat. Res., 92, 133–145, https://doi.org/10.1017/qua.2018.137, 2019b

Liu, Z., Zhu, J., Rosenthal, Y., Zhang, X., Otto-Bliesner, B. L., Timmermann, A., Smith, R. S., Lohmann, G., Zheng, W., and Elison Timm, O.: The Holocene temperature conundrum, Proc. Natl. Acad. Sci. USA, 111, E3501–E3505, https://doi.org/10.1073/pnas.1407229111, 2014a

Liu, Z., Wen, X., Brady, E. C., Otto-Bliesner, B., Yu, G., Lu, H., Cheng, H., Wang, Y., Zheng, W., Ding, Y., Edwards, R. L., Cheng, J., Liu, W., and Yang, H.: Chinese cave records and the East Asia Summer Monsoon, Quat. Sci. Rev., 83, 115–128, https://doi.org/10.1016/j.quascirev.2013.10.021, 2014b

Loader, N. J., Robertson, I., Barker, A. C., Switsur, V. R., and Waterhouse, J. S.: An improved technique for the batch processing of small wholewood samples to α-cellulose, Chem. Geol., 136, 313–317, https://doi.org/10.1016/S0009-2541(96)00133-7, 1997

Loisel, J. and Bunsen, M.: Abrupt fen-bog transition across southern Patagonia: Timing, causes, and impacts on carbon sequestration, Front. Ecol. Evol., 8, https://doi.org/10.3389/fevo.2020.00273, 2020

770   Loisel, J. and Yu, Z.: Recent acceleration of carbon accumulation in a boreal peatland, south central Alaska, J. Geophys. Res. Biogeosci., 118, 41–53, https://doi.org/10.1029/2012JG001978, 2013

Loisel, J., Garneau, M., and Hélie, J.-F.: Modern *Sphagnum* δ^{13}C signatures follow a surface moisture gradient in two boreal peat bogs, James Bay lowlands, Québec, J. Quat. Sci., 24, 209–214, https://doi.org/10.1002/jqs.1221, 2009

Loisel, J., Yu, Z., Beilman, D. W., Camill, P., Alm, J., Amesbury, M. J., Anderson, D., Andersson, S., Bochicchio, C., Barber, K., Belyea, L. R., Bunbury, J., Chambers, F. M., Charman, D. J., De Vleeschouwer, F., Fiałkiewicz-Kozieł, B.,
775   Finkelstein, S. A., Gałka, M., Garneau, M., Hammarlund, D., Hinchcliffe, W., Holmquist, J., Hughes, P., Jones, M. C., Klein, E. S., Kokfelt, U., Korhola, A., Kuhry, P., Lamarre, A., Lamentowicz, M., Large, D., Lavoie, M., MacDonald, G., Magnan, G., Mäkilä, M., Mallon, G., Mathijssen, P., Mauquoy, D., McCarroll, J., Moore, T. R., Nichols, J., O'Reilly, B., Oksanen, P., Packalen, M., Peteet, D., Richard, P. J., Robinson, S., Ronkainen, T., Rundgren, M., Sannel, A. B. K., Tarnocai, C., Thom, T., Tuittila, E.-S., Turetsky, M., Väliranta, M., van der Linden, M., van Geel, B., van Bellen, S., Vitt, D., Zhao, Y., and Zhou,
780   W.: A database and synthesis of northern peatland soil properties and Holocene carbon and nitrogen accumulation, Holocene, 24, 1028–1042, https://doi.org/10.1177/0959683614538073, 2014

Magnan, G., Sanderson, N. K., Piilo, S., Pratte, S., Väliranta, M., van Bellen, S., Zhang, H., and Garneau, M.: Widespread recent ecosystem state shifts in high-latitude peatlands of northeastern Canada and implications for carbon sequestration, Global Change Biol., 28, 1919–1934, https://doi.org/10.1111/gcb.16032, 2022

785   Magnan, G., van Bellen, S., Davies, L., Froese, D., Garneau, M., Mullan-Boudreau, G., Zaccone, C., and Shotyk, W.: Impact of the Little Ice Age cooling and 20th century climate change on peatland vegetation dynamics in central and northern Alberta using a multi-proxy approach and high-resolution peat chronologies, Quat. Sci. Rev., 185, 230–243, https://doi.org/10.1016/j.quascirev.2018.01.015, 2018

Manies, K. L., Jones, M. C., Waldrop, M. P., Leewis, M.-C., Fuller, C., Cornman, R. S., and Hoefke, K.: Influence of
790   permafrost type and site history on losses of permafrost carbon after thaw, J. Geophys. Res. Biogeosci., 126, e2021JG006396, https://doi.org/10.1029/2021JG006396, 2021

Miao, Y., Song, C., Sun, L., Wang, X., Meng, H., and Mao, R.: Growing season methane emission from a boreal peatland in the continuous permafrost zone of Northeast China: Effects of active layer depth and vegetation, Biogeosciences, 9, 4455–4464, https://doi.org/10.5194/bg-9-4455-2012, 2012a

795   Miao, Y., Song, C., Wang, X., Sun, X., Meng, H., and Sun, L.: Greenhouse gas emissions from different wetlands during the snow-covered season in Northeast China, Atmos. Environ., 62, 328–335, https://doi.org/10.1016/j.atmosenv.2012.08.036, 2012b

Morris, P. J., Baird, A. J., Young, D. M., and Swindles, G. T.: Untangling climate signals from autogenic changes in long-term peatland development, Geophys. Res. Lett., 42, 10788–10797, https://doi.org/10.1002/2015GL066824, 2015

800   Morris, P. J., Swindles, G. T., Valdes, P. J., Ivanovic, R. F., Gregoire, L. J., Smith, M. W., Tarasov, L., Haywood, A. M., and Bacon, K. L.: Global peatland initiation driven by regionally asynchronous warming, Proc. Natl. Acad. Sci. USA, 115, 4851–4856, https://doi.org/10.1073/pnas.1717838115, 2018

O'Donnell, J. A., Jorgenson, M. T., Harden, J. W., McGuire, A. D., Kanevskiy, M. Z., and Wickland, K. P.: The effects of permafrost thaw on soil hydrologic, thermal, and carbon dynamics in an Alaskan peatland, Ecosystems, 15, 213–229,
805   https://doi.org/10.1007/s10021-011-9504-0, 2012

Oksanen, P. O., Kuhry, P., and Alekseeva, R. N.: Holocene development of the Rogovaya River peat plateau, European Russian Arctic, Holocene, 11, 25–40, https://doi.org/10.1191/095968301675477157, 2001

Olefeldt, D. and Roulet, N. T.: Permafrost conditions in peatlands regulate magnitude, timing, and chemical composition of catchment dissolved organic carbon export, Global Change Biol., 20, 3122–3136, https://doi.org/10.1111/gcb.12607, 2014

810 Olefeldt, D., Heffernan, L., Jones, M. C., Sannel, A. B. K., Treat, C. C., and Turetsky, M. R.: Permafrost thaw in northern peatlands: Rapid changes in ecosystem and landscape functions, in: Ecosystem Collapse and Climate Change, edited by: Canadell, J. G., and Jackson, R. B., Springer Nature Switzerland, Cham, Switzerland, 27–67, https://doi.org/10.1007/978-3-030-71330-0_3, 2021.

Olefeldt, D., Goswami, S., Grosse, G., Hayes, D., Hugelius, G., Kuhry, P., McGuire, A. D., Romanovsky, V. E., Sannel, A.
815 B. K., Schuur, E. A. G., and Turetsky, M. R.: Circumpolar distribution and carbon storage of thermokarst landscapes, Nat. Commun., 7, 13043, https://doi.org/10.1038/ncomms13043, 2016

Park, H., Launiainen, S., Konstantinov, P. Y., Iijima, Y., and Fedorov, A. N.: Modeling the effect of moss cover on soil temperature and carbon fluxes at a tundra site in northeastern Siberia, J. Geophys. Res. Biogeosci., 123, 3028–3044, https://doi.org/10.1029/2018JG004491, 2018

820 Payette, S., Delwaide, A., Caccianiga, M., and Beauchemin, M.: Accelerated thawing of subarctic peatland permafrost over the last 50 years, Geophys. Res. Lett., 31, L18208, https://doi.org/10.1029/2004GL020358, 2004

Piilo, S. R., Väliranta, M. M., Amesbury, M. J., Aquino-López, M. A., Charman, D. J., Gallego-Sala, A., Garneau, M., Koroleva, N., Kärppä, M., Laine, A. M., Sannel, A. B. K., Tuittila, E.-S., and Zhang, H.: Consistent centennial-scale change in European sub-Arctic peatland vegetation toward *Sphagnum* dominance—Implications for carbon sink capacity, Global
825 Change Biol., 29, 1530–1544, https://doi.org/10.1111/gcb.16554, 2023

Quik, C., van der Velde, Y., Candel, J. H. J., Steinbuch, L., van Beek, R., and Wallinga, J.: Faded landscape: unravelling peat initiation and lateral expansion at one of northwest Europe's largest bog remnants, Biogeosciences, 20, 695–718, https://doi.org/10.5194/bg-20-695-2023, 2023

Ramm, E., Liu, C., Mueller, C. W., Gschwendtner, S., Yue, H., Wang, X., Bachmann, J., Bohnhoff, J. A., Ostler, U.,
830 Schloter, M., Rennenberg, H., and Dannenmann, M.: Alder-induced stimulation of soil gross nitrogen turnover in a permafrost-affected peatland of Northeast China, Soil Biol. Biochem., 172, 108757, https://doi.org/10.1016/j.soilbio.2022.108757, 2022

Ran, Y., Li, X., Cheng, G., Zhang, T., Wu, Q., Jin, H., and Jin, R.: Distribution of permafrost in China: An overview of existing permafrost maps, Permafr. Periglac. Process., 23, 322–333, https://doi.org/10.1002/ppp.1756, 2012

835 Rice, S. K. and Giles, L.: The influence of water content and leaf anatomy on carbon isotope discrimination and photosynthesis in *Sphagnum*, Plant Cell Environ., 19, 118–124, https://doi.org/10.1111/j.1365-3040.1996.tb00233.x, 1996

Risi, C., Bony, S., Vimeux, F., and Jouzel, J.: Water-stable isotopes in the LMDZ4 general circulation model: Model evaluation for present-day and past climates and applications to climatic interpretations of tropical isotopic records, J. Geophys. Res., 115, D12118, https://doi.org/10.1029/2009JD013255, 2010

840 Robinson, S. D. and Moore, T. R.: The influence of permafrost and fire upon carbon accumulation in high boreal peatlands, Northwest Territories, Canada, Arct. Antarct. Alp. Res., 32, 155–166, http://doi.org/10.1080/15230430.2000.12003351, 2000

Ruppel, M., Väliranta, M., Virtanen, T., and Korhola, A.: Postglacial spatiotemporal peatland initiation and lateral expansion dynamics in North America and northern Europe, Holocene, 23, 1596-1606, https://doi.org/10.1177/0959683613499053,
845   2013

Rydin, H. and Jeglum, J. K.: The Biology of Peatlands (2nd Edition), Oxford University Press, Oxford, UK, 2013.

Sannel, A. B. K. and Kuhry, P.: Holocene peat growth and decay dynamics in sub-arctic peat plateaus, west-central Canada, Boreas, 38, 13–24, https://doi.org/10.1111/j.1502-3885.2008.00048.x, 2009

Scheffer, M. and Carpenter, S. R.: Catastrophic regime shifts in ecosystems: linking theory to observation, Trends Ecol.
850   Evol., 18, 648–656, https://doi.org/10.1016/j.tree.2003.09.002, 2003

Schneider von Deimling, T., Meinshausen, M., Levermann, A., Huber, V., Frieler, K., Lawrence, D. M., and Brovkin, V.: Estimating the near-surface permafrost-carbon feedback on global warming, Biogeosciences, 9, 649–665, https://doi.org/10.5194/bg-9-649-2012, 2012

Sim, T. G., Swindles, G. T., Morris, P. J., Gałka, M., Mullan, D., and Galloway, J. M.: Pathways for ecological change in
855   Canadian high Arctic wetlands under rapid twentieth century warming, Geophys. Res. Lett., 46, 4726–4737, https://doi.org/10.1029/2019GL082611, 2019

Sim, T. G., Swindles, G. T., Morris, P. J., Baird, A. J., Cooper, C. L., Gallego-Sala, A. V., Charman, D. J., Roland, T. P., Borken, W., Mullan, D. J., Aquino-López, M. A., and Gałka, M.: Divergent responses of permafrost peatlands to recent climate change, Environ. Res. Lett., 16, 034001, http://doi.org/10.1088/1748-9326/abe00b, 2021

860   Smith, L. C., Sheng, Y., and MacDonald, G. M.: A first pan-Arctic assessment of the influence of glaciation, permafrost, topography and peatlands on northern hemisphere lake distribution, Permafr. Periglac. Process., 18, 201–208, https://doi.org/10.1002/ppp.581, 2007

Sun, G.: Discussion on the symbiotic mechanisms of swamp with permafrost, Journal of Glaciology and Geocryology, 22, 309–316, 2000 (in Chinese with an English abstract).

865   Sun, L., Song, C., Lafleur, P. M., Wang, X., Tan, W., Du, Y., Qiao, T., and Wang, Y.: Multi-scale temporal variation in CH_4 and CO_2 exchange and associated biophysical controls from two wetlands in Northeast China, Agric. For. Meteorol., 345, 109818, https://doi.org/10.1016/j.agrformet.2023.109818, 2024

Swindles, G. T., Morris, P. J., Mullan, D., Watson, E. J., Turner, T. E., Roland, T. P., Amesbury, M. J., Kokfelt, U., Schoning, K., Pratte, S., Gallego-Sala, A., Charman, D. J., Sanderson, N., Garneau, M., Carrivick, J. L., Woulds, C., Holden,
870   J., Parry, L., and Galloway, J. M.: The long-term fate of permafrost peatlands under rapid climate warming, Sci. Rep., 5, 17951, https://doi.org/10.1038/srep17951, 2015

Taylor, L. S., Swindles, G. T., Morris, P. J., Gałka, M., and Green, S. M.: Evidence for ecosystem state shifts in Alaskan continuous permafrost peatlands in response to recent warming, Quat. Sci. Rev., 207, 134–144, https://doi.org/10.1016/j.quascirev.2019.02.001, 2019

875   Treat, C. C., Jones, M. C., Alder, J., Sannel, A. B. K., Camill, P., and Frolking, S.: Predicted vulnerability of carbon in permafrost peatlands with future climate change and permafrost thaw in western Canada, J. Geophys. Res. Biogeosci., 126, e2020JG005872, https://doi.org/10.1029/2020JG005872, 2021

Treat, C. C., Wollheim, W. M., Varner, R. K., Grandy, A. S., Talbot, J., and Frolking, S.: Temperature and peat type control CO_2 and CH_4 production in Alaskan permafrost peats, Global Change Biol., 20, 2674–2686,
880 https://doi.org/10.1111/gcb.12572, 2014

Treat, C. C., Jones, M. C., Camill, P., Gallego-Sala, A., Garneau, M., Harden, J. W., Hugelius, G., Klein, E. S., Kokfelt, U., Kuhry, P., Loisel, J., Mathijssen, P. J. H., O'Donnell, J. A., Oksanen, P. O., Ronkainen, T. M., Sannel, A. B. K., Talbot, J., Tarnocai, C., and Väliranta, M.: Effects of permafrost aggradation on peat properties as determined from a pan-Arctic synthesis of plant macrofossils, J. Geophys. Res. Biogeosci., 121, 78–94, https://doi.org/10.1002/2015JG003061, 2016

885 Treat, C. C., Kleinen, T., Broothaerts, N., Dalton, A. S., Dommain, R., Douglas, T. A., Drexler, J. Z., Finkelstein, S. A., Grosse, G., Hope, G., Hutchings, J., Jones, M. C., Kuhry, P., Lacourse, T., Lähteenoja, O., Loisel, J., Notebaert, B., Payne, R. J., Peteet, D. M., Sannel, A. B. K., Stelling, J. M., Strauss, J., Swindles, G. T., Talbot, J., Tarnocai, C., Verstraeten, G., Williams, C. J., Xia, Z., Yu, Z., Väliranta, M., Hättestrand, M., Alexanderson, H., and Brovkin, V.: Widespread global peatland establishment and persistence over the last 130,000 y, Proc. Natl. Acad. Sci. USA, 116, 4822–4827,
890 https://doi.org/10.1073/pnas.1813305116, 2019

Turetsky, M. R., Wieder, R. K., and Vitt, D. H.: Boreal peatland C fluxes under varying permafrost regimes, Soil Biol. Biochem., 34, 907–912, https://doi.org/10.1016/S0038-0717(02)00022-6, 2002

Turetsky, M. R., Wieder, R. K., Vitt, D. H., Evans, R. J., and Scott, K. D.: The disappearance of relict permafrost in boreal north America: Effects on peatland carbon storage and fluxes, Global Change Biol., 13, 1922–1934,
895 https://doi.org/10.1111/j.1365-2486.2007.01381.x, 2007

Turetsky, M. R., Abbott, B. W., Jones, M. C., Anthony, K. W., Olefeldt, D., Schuur, E. A. G., Grosse, G., Kuhry, P., Hugelius, G., Koven, C., Lawrence, D. M., Gibson, C., Sannel, A. B. K., and McGuire, A. D.: Carbon release through abrupt permafrost thaw, Nat. Geosci., 13, 138–143, https://doi.org/10.1038/s41561-019-0526-0, 2020

van Breemen, N.: How *Sphagnum* bogs down other plants, Trends Ecol. Evol., 10, 270–275, https://doi.org/10.1016/0169-
900 5347(95)90007-1, 1995

Vitt, D. H., Halsey, L. A., and Zoltai, S. C.: The bog landforms of continental western Canada in relation to climate and permafrost patterns, Arct. Alp. Res., 26, 1–13, http://doi.org/10.1080/00040851.1994.12003032, 1994

Vitt, D. H., Halsey, L. A., and Zoltai, S. C.: The changing landscape of Canada's western boreal forest: The current dynamics of permafrost, Can. J. For. Res., 30, 283–287, https://doi.org/10.1139/x99-214, 2000

905 Voigt, C., Marushchak, M. E., Lamprecht, R. E., Jackowicz-Korczyński, M., Lindgren, A., Mastepanov, M., Granlund, L., Christensen, T. R., Tahvanainen, T., Martikainen, P. J., and Biasi, C.: Increased nitrous oxide emissions from Arctic peatlands after permafrost thaw, Proc. Natl. Acad. Sci. USA, 114, 6238–6243, https://doi.org/10.1073/pnas.1702902114, 2017

Voigt, C., Marushchak, M. E., Mastepanov, M., Lamprecht, R. E., Christensen, T. R., Dorodnikov, M., Jackowicz-
910 Korczyński, M., Lindgren, A., Lohila, A., Nykänen, H., Oinonen, M., Oksanen, T., Palonen, V., Treat, C. C., Martikainen, P. J., and Biasi, C.: Ecosystem carbon response of an Arctic peatland to simulated permafrost thaw, Global Change Biol., 25, 1746–1764, https://doi.org/10.1111/gcb.14574, 2019

Waddington, J. M., Morris, P. J., Kettridge, N., Granath, G., Thompson, D. K., and Moore, P. A.: Hydrological feedbacks in northern peatlands, Ecohydrol., 8, 113–127, https://doi.org/10.1002/eco.1493, 2015

915 Wang, X., Li, X., Hu, Y., Lv, J., Sun, J., Li, Z., and Wu, Z.: Effect of temperature and moisture on soil organic carbon mineralization of predominantly permafrost peatland in the Great Hing'an Mountains, Northeastern China, J. Environ. Sci., 22, 1057–1066, https://doi.org/10.1016/S1001-0742(09)60217-5, 2010

Wang, Y., Cheng, H., Edwards, R. L., He, Y., Kong, X., An, Z., Wu, J., Kelly, M. J., Dykoski, C. A., and Li, X.: The Holocene Asian monsoon: Links to solar changes and North Atlantic climate, Science, 308, 854–857,
920 https://doi.org/10.1126/science.1106296, 2005

Weckström, J., Seppä, H., and Korhola, A.: Climatic influence on peatland formation and lateral expansion in sub-arctic Fennoscandia, Boreas, 39, 761–769, https://doi.org/10.1111/j.1502-3885.2010.00168.x, 2010

Wen, R., Xiao, J., Chang, Z., Zhai, D., Xu, Q., Li, Y., and Itoh, S.: Holocene precipitation and temperature variations in the East Asian monsoonal margin from pollen data from Hulun Lake in northeastern Inner Mongolia, China, Boreas, 39, 262–
925 272, https://doi.org/10.1111/j.1502-3885.2009.00125.x, 2010

Williams, T. G. and Flanagan, L. B.: Effect of changes in water content on photosynthesis, transpiration and discrimination against $^{13}CO_2$ and $C^{18}O^{16}O$ in *Pleurozium* and *Sphagnum*, Oecologia, 108, 38–46, https://doi.org/10.1007/BF00333212, 1996

Xia, Y., Yang, Z., Sun, J., Xia, Z., and Yu, Z.: Late-Holocene ecosystem dynamics and climate sensitivity of a permafrost peatland in Northeast China, Quat. Sci. Rev., 324, 108466, https://doi.org/10.1016/j.quascirev.2023.108466, 2024a

930 Xia, Z., Yang, W., and Yu, Z.: Major moisture shifts in inland Northeast Asia during the last millennium, Environ. Res. Lett., 19, 124005, https://doi.org/10.1088/1748-9326/ad8763, 2024b

Xia, Z., Yu, Z., and Loisel, J.: Centennial-scale dynamics of the Southern Hemisphere Westerly Winds across the Drake Passage over the past two millennia, Geology, 46, 855–858, https://doi.org/10.1130/G40187.1, 2018

Xia, Z., Zheng, Y., Stelling, J. M., Loisel, J., Huang, Y., and Yu, Z.: Environmental controls on the carbon and water (H and
935 O) isotopes in peatland *Sphagnum* mosses, Geochim. Cosmochim. Acta, 277, 265–284, https://doi.org/10.1016/j.gca.2020.03.034, 2020

Xing, W., Bao, K., Guo, W., Lu, X., and Wang, G.: Peatland initiation and carbon dynamics in northeast China: Links to Holocene climate variability, Boreas, 44, 575–587, https://doi.org/10.1111/bor.12116, 2015

Xu, J., Morris, P. J., Liu, J., and Holden, J.: PEATMAP: Refining estimates of global peatland distribution based on a meta-
940 analysis, Catena, 160, 134–140, https://doi.org/10.1016/j.catena.2017.09.010, 2018

Yang, Y.: Study on formation and development of forest swamp and paleoenvironment change since the Holocene in the east part of the Xiaoxinganling Mountains, Oceanologia et Limnologia Sinica, 34, 74–82, 2003 (in Chinese with an English abstract).

Yao, Y., Huang, Y., Zhao, J., Wang, L., Ran, Y., Liu, W., and Cheng, H.: Permafrost thaw induced abrupt changes in
945 hydrology and carbon cycling in Lake Wudalianchi, northeastern China, Geology, 49, 1117–1121, https://doi.org/10.1130/G48891.1, 2021

Yoshimura, K., Kanamitsu, M., Noone, D., and Oki, T.: Historical isotope simulation using reanalysis atmospheric data, J. Geophys. Res., 113, D19108, https://doi.org/10.1029/2008JD010074, 2008

Young, D. M., Baird, A. J., Gallego-Sala, A. V., and Loisel, J.: A cautionary tale about using the apparent carbon
950 accumulation rate (aCAR) obtained from peat cores, Sci. Rep., 11, 9547, https://doi.org/10.1038/s41598-021-88766-8, 2021

Young, D. M., Baird, A. J., Charman, D. J., Evans, C. D., Gallego-Sala, A. V., Gill, P. J., Hughes, P. D. M., Morris, P. J., and Swindles, G. T.: Misinterpreting carbon accumulation rates in records from near-surface peat, Sci. Rep., 9, 17939, https://doi.org/10.1038/s41598-019-53879-8, 2019

Yu, X., Song, C., Sun, L., Wang, X., Shi, F., Cui, Q., and Tan, W.: Growing season methane emissions from a permafrost peatland of northeast China: Observations using open-path eddy covariance method, Atmos. Environ., 153, 135–149, https://doi.org/10.1016/j.atmosenv.2017.01.026, 2017

Yu, Z., Beilman, D. W., and Jones, M. C.: Sensitivity of northern peatland carbon dynamics to Holocene climate change, in: Carbon Cycling in Northern Peatlands (Geophysical Monograph Series), edited by: Baird, A. J., Belyea, L. R., Comas, X., Reeve, A. S., and Slater, L. D., American Geophysical Union, Washington, DC, USA, 55–69, 2009.

Yu, Z., Turetsky, M. R., Campbell, I. D., and Vitt, D. H.: Modelling long-term peatland dynamics. II. Processes and rates as inferred from litter and peat-core data, Ecol. Model., 145, 159–173, https://doi.org/10.1016/S0304-3800(01)00387-8, 2001

Yu, Z., Loisel, J., Brosseau, D. P., Beilman, D. W., and Hunt, S. J.: Global peatland dynamics since the Last Glacial Maximum, Geophys. Res. Lett., 37, L13402, https://doi.org/10.1029/2010GL043584, 2010

Yu, Z., Beilman, D. W., Frolking, S., MacDonald, G. M., Roulet, N. T., Camill, P., and Charman, D. J.: Peatlands and their role in the global carbon cycle, Eos. Trans. AGU, 92, 97–98, https://doi.org/10.1029/2011EO120001, 2011

Yu, Z. C.: Northern peatland carbon stocks and dynamics: a review, Biogeosciences, 9, 4071–4085, https://doi.org/10.5194/bg-9-4071-2012, 2012

Zhang, F., Cheng, J., Sun, W., Meng, X., Ni, Z., Wang, Y., and Zhang, E.: Mid-late Holocene meridional out-of-phase precipitation patterns in the margin of the East Asian monsoon region revealed by paleoclimate records and simulations, Quat. Sci. Rev., 352, 109211, https://doi.org/10.1016/j.quascirev.2025.109211, 2025

Zhang, H., Gallego-Sala, A. V., Amesbury, M. J., Charman, D. J., Piilo, S. R., and Väliranta, M. M.: Inconsistent response of Arctic permafrost peatland carbon accumulation to warm climate phases, Global Biogeochem. Cycles, 32, 1605–1620, https://doi.org/10.1029/2018GB005980, 2018a

Zhang, H., Piilo, S. R., Amesbury, M. J., Charman, D. J., Gallego-Sala, A. V., and Väliranta, M. M.: The role of climate change in regulating Arctic permafrost peatland hydrological and vegetation change over the last millennium, Quat. Sci. Rev., 182, 121–130, https://doi.org/10.1016/j.quascirev.2018.01.003, 2018b

Zhang, H., Väliranta, M., Piilo, S., Amesbury, M. J., Aquino-López, M. A., Roland, T. P., Salminen-Paatero, S., Paatero, J., Lohila, A., and Tuittila, E.-S.: Decreased carbon accumulation feedback driven by climate-induced drying of two southern boreal bogs over recent centuries, Global Change Biol., 26, 2435–2448, https://doi.org/10.1111/gcb.15005, 2020a

Zhang, H., Väliranta, M., Swindles, G. T., Aquino-López, M. A., Mullan, D., Tan, N., Amesbury, M., Babeshko, K. V., Bao, K., Bobrov, A., Chernyshov, V., Davies, M. A., Diaconu, A.-C., Feurdean, A., Finkelstein, S. A., Garneau, M., Guo, Z., Jones, M. C., Kay, M., Klein, E. S., Lamentowicz, M., Magnan, G., Marcisz, K., Mazei, N., Mazei, Y., Payne, R., Pelletier, N., Piilo, S. R., Pratte, S., Roland, T., Saldaev, D., Shotyk, W., Sim, T. G., Sloan, T. J., Słowiński, M., Talbot, J., Taylor, L., Tsyganov, A. N., Wetterich, S., Xing, W., and Zhao, Y.: Recent climate change has driven divergent hydrological shifts in high-latitude peatlands, Nat. Commun., 13, 4959, https://doi.org/10.1038/s41467-022-32711-4, 2022

Zhang, M., Bu, Z., Wang, S., and Jiang, M.: Moisture changes in Northeast China since the last deglaciation: Spatiotemporal out-of-phase patterns and possible forcing mechanisms, Earth Sci. Rev., 201, 102984, https://doi.org/10.1016/j.earscirev.2019.102984, 2020b

Zhang, X.-M., Chen, L., Ji, J.-Z., Wang, J., Wang, Y.-B., Guo, W., and Lan, B.-W.: Climate change and its effect in Harbin
990   from 1881 to 2010, Journal of Meteorology and Environment, 27, 13–20, 2011 (in Chinese with an English abstract).

Zhang, Z.-Q., Wu, Q.-B., Hou, M.-T., Tai, B.-W., and An, Y.-K.: Permafrost change in Northeast China in the 1950s–2010s,
Adv. Clim. Change Res., 12, 18–28, https://doi.org/10.1016/j.accre.2021.01.006, 2021

Zhou, X., Sun, L., Zhan, T., Huang, W., Zhou, X., Hao, Q., Wang, Y., He, X., Zhao, C., Zhang, J., Qiao, Y., Ge, J., Yan, P.,
Yan, Q., Shao, D., Chu, Z., Yang, W., and Smol, J. P.: Time-transgressive onset of the Holocene Optimum in the East Asian
995   monsoon region, Earth Planet. Sci. Lett., 456, 39–46, https://doi.org/10.1016/j.epsl.2016.09.052, 2016

Zoltai, S. C.: Cyclic development of permafrost in the peatlands of northwestern Alberta, Canada, Arct. Alp. Res., 25, 240–
246, https://doi.org/10.1080/00040851.1993.12003011, 1993

Zoltai, S. C. and Tarnocai, C.: Perennially frozen peatlands in the western Arctic and subarctic of Canada, Can. J. Earth Sci.,
12, 28–43, https://doi.org/10.1139/e75-004, 1975
1000